Title
Fluorogenic reporter enables identification of compounds that inhibit SARS-CoV-2

Journal
Nature Microbiology, 8(1)

ISSN
2058-5276

Authors
Yang, Junjiao
Xiao, Yinghong
Lidsky, Peter V
et al.

Publication Date
2023

DOI
10.1038/s41564-022-01288-5

Peer reviewed

HHS Public Access

Author manuscript

Nat Microbiol. Author manuscript; available in PMC 2023 July 05.

Published in final edited form as:

Nat Microbiol. 2023 January ; 8(1): 121–134. doi:10.1038/s41564-022-01288-5.

Fluorogenic reporter enables identification of compounds that inhibit SARS-CoV-2

Junjiao Yang[1,2,#], **Yinghong Xiao**[3,#], **Peter V. Lidsky**[3,#], **Chien-Ting Wu**[4], **Luke R. Bonser**[5], **Shiming Peng**[1], **Miguel A. Garcia-Knight**[3], **Michel Tassetto**[3], **Chan-I Chung**[1,2], **Xiaoquan Li**[1,2], **Tsuguhisa Nakayama**[6], **Ivan T. Lee**[7], **Jayakar V. Nayak**[6,8], **Khadija Ghias**[5], **Kirsten L. Hargett**[5], **Brian K. Shoichet**[1], **David J. Erle**[5], **Peter K. Jackson**[4], **Raul Andino**[3,*], **Xiaokun Shu**[1,2,*]

[1]Department of Pharmaceutical Chemistry, University of California, San Francisco, San Francisco, California, USA.

[2]Cardiovascular Research Institute, University of California, San Francisco, San Francisco, California, USA

[3]Department of Microbiology and Immunology, University of California, San Francisco, San Francisco, California, USA.

[4]Department of Baxter Laboratory for Stem Cell Biology, Department of Microbiology & Immunology, Stanford University, California, USA

[5]Lung Biology Center, Department of Medicine, University of California, San Francisco, San Francisco, California, USA

[6]Department of Otolaryngology–Head and Neck Surgery, Stanford University, Stanford, California, USA

[7]Division of Allergy, Immunology, and Rheumatology, Department of Pediatrics, Stanford University School of Medicine, Stanford, CA, USA.

[8]Department of Otolaryngology–Head and Neck Surgery, VA Palo Alto Health Care System, Palo Alto, CA USA

[*]Correspondence to: Raul Andino: raul.andino@ucsf.edu, Xiaokun Shu, xiaokun.shu@ucsf.edu.
[#]These authors contributed to the work equally.

Author contributions: J.Y. and X.S. initiated the project and designed the fluorescent reporters and assays. J.Y., C-I.C., and X.L. prepared the drug and natural compound library. J.Y. performed screens and characterized kinetics of PPI inhibition in cells. Y.X., P.L., and R.A. designed SARS-CoV-2 BSL3 experiments in cells and animals and interpreted the data. Y.X. and P.L. performed plaque assays and calculated plaque numbers, and J.Y., Y.X., and P.L. performed quantitative analysis and plotted data. M.K. isolated virus variants, performed RT-qPCR and analyzed the data. J.Y. performed toxicity assays. P.L. and Y.X. infected Vero cells, and J.Y. performed immunostaining and analyzed immunofluorescence. Y.X., P.L., T.N., J.V.N., C.W., P. K. J., and R.A. designed the HNEpC infection experiments. Y.X. and P.L. performed viral infection, C.W., T.N., and I.T.L. performed cell culturing, C.W. conducted immunostaining and imaging, J.Y. and X.L. performed quantitative analysis. J.Y. and L.R.B. designed HBEpC infection experiments, L.R.B. and K.G. performed HBEpC culturing, P.L. and M.T. performed viral infection, J.Y. performed immunostaining, imaging, and quantitative analysis. S.P., B.K.S. performed and analyzed molecular docking. X.S., J.Y., Y.X. wrote the manuscript, and J.Y., Y.X., P.L., M.K., C.W., S.P., M.T. wrote the methods. All authors edited and contributed to the final draft.

Competing interests:
The authors declare the following competing interest: J.Y. and X.S. have filed a patent on the imaging assay.

Supplementary Information:
supplementary Figs. S1–12
source data for supplementary figures

Abstract

The coronavirus SARS-CoV-2 causes the severe disease COVID-19. SARS-CoV-2 infection is initiated by the interaction of the viral spike protein and the host receptor angiotensin-converting enzyme 2 (ACE2). We report an improved bright and reversible fluorogenic reporter named SURF (Split UnaG-based Reversible and Fluorogenic PPI reporter) which we apply to monitor real-time interactions between spike and ACE2 in living cells. SURF has a large dynamic range with a dark-to-bright fluorescence signal that requires no exogenous cofactors. Utilizing this reporter, we carried out a high-throughput screening of small-molecule libraries. We identified three natural compounds that block replication of SARS-CoV-2 in Vero cells, and in human primary nasal and bronchial epithelial cells. Cell biological and biochemical experiments validated all three compounds and showed that they block the early stages of viral infection. Two of the inhibitors, bruceine A and gamabufotalin, were also found to block replication of the Delta and Omicron variants of SARS-CoV-2. Both bruceine A and gamabufotalin exhibited potent antiviral activity in K18-hACE2 and wild-type C57BL6/J mice, as evidenced by reduced viral titres in the lung and brain, and protection from alveolar and peribronchial inflammation in the lung, thereby limiting disease progression. We propose that our fluorescent assay can be applied to identify antiviral compounds with potential as therapeutic treatment for COVID-19 and other respiratory diseases.

Introduction

The worldwide pandemic of the respiratory disease COVID-19 caused by the coronavirus SARS-CoV-2 (severe acute respiratory syndrome coronavirus 2) has produced huge health challenges and economic loss. While effective vaccines and therapeutic monoclonal antibodies are available, a large part of the global population remains unvaccinated and without access to monoclonal therapies due to their cost and limited supply [1,2]. Moreover, immune escape mutations in the spike (S) protein may weaken the efficacy of current interventions [3]. Thus, small-molecule drugs are urgently needed to curb the progression of the COVID-19 pandemic.

The first step in the entry of SARS-CoV-2 into human cells is viral binding to the host cell, which is achieved by protein-protein interaction (PPI) between the virus surface-anchored S protein and the host cell receptor angiotensin-converting enzyme 2 (ACE2) [4–7]. The trimeric S protein is cleaved into S1 and S2 subunits. The S1 subunit contains a receptor-binding domain (RBD) that binds the extracellular peptidase domain (PD) of ACE2. The coronavirus enters into the host cells [8,9], and the viral genomic RNA is released into the cytoplasm. After viral RNA replication, mature virions are assembled and released via budding from the host cells.

Therefore, inhibiting the PPI between the S protein and ACE2 may block the entry of SARS-CoV-2 into human cells, prevent infection and ultimately remedy COVID-19 disease. Indeed, this PPI is a major target for therapeutic intervention, and researchers have developed antibodies, *de novo* designed proteins, peptides, and engineered ACE2 to bind the S protein and inhibit viral binding and infection [10–13]. Here we report the identification of small-molecule inhibitors, including natural compounds, that block the S-ACE2 interaction,

inhibit binding of SARS-CoV-2 to cells, and potently suppress replication of the coronavirus in the host cells.

We identified the inhibitors using a reversible and fluorogenic PPI reporter that enables direct visualization of spike and ACE2 interactions in living cells. This PPI reporter has large dynamic range with dark-to-bright fluorescence signal that requires no exogenous cofactors. It visualizes the interaction between spike protein and its receptor ACE2. And it is generalizable to imaging interaction of spike with other receptors such as neuropillin-1. Two of the identified natural products using this method potently inhibit replication of SARS-CoV-2 in vivo and might be developed into antiviral therapeutics for treating COVID-19.

Results

Engineering reporters for imaging Spike and ACE2 interactions

To design a fluorogenic reporter for detecting the interaction between the S protein and ACE2, we improved a green fluorescent PPI reporter we previously engineered from UnaG [14,15]. We named this PPI reporter SURF (Split UnaG-based Reversible and Fluorogenic PPI reporter). Like its parent protein UnaG, SURF incorporates endogenous bilirubin as the chromophore, and thus, its genetically encoded fluorescence does not require an exogenous cofactor. To visualize the interaction of two proteins, we fuse each fragment of SURF (cSURF: carboxyl-terminal fragment; nSURF: amino-terminal fragment) to the proteins of interest (Fig. 1A). When interactions of the two proteins bring the two fragments into close proximity, the two parts of SURF reconstitute and become fluorescent (Fig. 1A, supplementary Fig. S1). Because SURF is reversible, inhibition of PPI leads to dissociation of the two fragments of SURF, resulting in no fluorescence.

Next, we applied SURF to design PPI reporters of the S protein and ACE2 interaction by structure-based protein design and engineering. Crystal structures of complexes of the S protein, ACE2 and B^0AT1 revealed that the PPI of S and ACE2 is mediated by the receptor-binding domain of the S protein (S^{RBD}) [4–7]. Thus, we fused C- and N-terminal components of SURF, i.e. cSURF and nSURF, to S^{RBD} and ACE2, respectively (Fig. 1B). The interaction of S^{RBD} and ACE2 brings the two fragments of SURF into close proximity so that SURF reconstitutes and becomes fluorescent. Disruption of the S^{RBD}::ACE2 interaction leads to dissociation of the two SURF fragments, resulting loss of fluorescence. To design the two parts of the SURF reporter into one construct, we utilized the “self-cleaving” 2A peptide [16] (Fig. 1C, upper left). We expressed this initial SURF reporter in human embryonic kidney 293T (HEK293T) cells (Fig. 1C, lower left), which showed green fluorescence as expected, though the fluorescence was dim.

To make the reporter more suitable for high-throughput screening (HTS), we used structure-guided protein engineering, which increased its brightness ~270-fold (Fig. 1C, right panel; Fig. 1D). In particular, we engineered ACE2 by truncating the C-terminal fragment of ACE2 and found that removing residues 616–727 improved the brightness by 2.2-fold (Fig. 1D). We then shortened the N-terminal fragment of ACE2 by removing residues 1–16, which further increased the brightness 3.5-fold. The truncated ACE2, including residues 17–615, was named as ΔACE2. Truncating S^{RBD} did not improve brightness. We next

incorporated a red fluorescent protein mCherry[17–19] into our reporter to normalize the green fluorescence of SURF. We placed mCherry between S^{RBD} and cSURF, which surprisingly improved SURF brightness by 30-fold (Fig. 1D). The mCherry likely functions as a spacer between S^{RBD} and cSURF that may assist SURF reconstitution upon association of S^{RBD} and ΔACE2. A 2nd mCherry between nSURF and ΔACE2 further improved the brightness, leading to a SURF reporter 270-fold brighter than the initial reporter. We named this variant of SURF reporter S^{RBD}::ΔACE2 SURF (for simplicity, the two incorporated mCherry moieties are not shown).

Next, we examined reversibility of the S^{RBD}::ΔACE2 SURF system. S^{RBD} or ΔACE2 (each fused to a near-infrared fluorescence protein IFP2) [20,21] was co-expressed to compete against S^{RBD}-cSURF or ΔACE2-nSURF, respectively, which would inhibit SURF reconstitution. SURF fluorescence was abolished, whereas mCherry fluorescence was stable (Fig. 1E, supplementary Fig. S2). As a control, IFP2 expression did not perturb SURF fluorescence. Quantification of the results and calculation of a *Z-factor* [22]

$$Z = 1 - \frac{(3\sigma_+ + 3\sigma_-)}{|u_+ - u_-|},$$

gave us ~0.7 with IFP2 and IFP2 fusion to S^{RBD} (or ΔACE2) as positive (+) and negative (−) controls of the S and ACE2 PPI, respectively (here σ is standard deviation, μ is mean). This indicates that the S^{RBD}::ΔACE2 SURF is a highly robust and versatile assay for HTS of PPI inhibitors that block S and ACE2 interaction in HEK293T cells. Thus, SURF-based approach enabled us to conduct HTS in living cells in biosafety level 2 (BSL-2).

Screening PPI inhibitors of Spike and ACE2 using SURF

Using the S^{RBD}::ΔACE2 SURF assay, we screened libraries of 1516 FDA-approved drugs and 2592 natural compounds (Fig. 2A, Extended Data Fig. 1A). First, the reporter was transfected into HEK293T cells, and the compounds were added and incubated for 24 hours. Next, we imaged the SURF and mCherry fluorescence of the cells. The degree of PPI inhibition was calculated based on SURF fluorescence normalized by mCherry. From the FDA-approved drug library, 15 drugs showed > 40% PPI inhibition with a p-value < 0.01 (Extended Data Fig. 1B). For the natural compound library, 52 compounds had > 50% PPI inhibition with a p-value < 0.01 (Fig. 2B).

To confirm the inhibitory activity of the FDA-approved drugs, an independent imaging of 15 drugs was conducted under the same condition. We selected the top 10 drugs (Extended Data Fig. 1C) and characterized their inhibition kinetics by time-lapse imaging using SURF. Seven drugs inhibited the PPI within 6 hours (Extended Data Fig. 1D), which were selected for antiviral activity measurement (see below). Lastly, the drugs showed little effect on a SURF control where cSURF and nSURF were directly linked together, suggesting that they have little effect on the reporter itself (supplementary Fig. S3).

For the identified natural compounds, their activity was confirmed by a second round of imaging (supplementary Fig. S4). Next, we narrowed the hits by shortening incubation time to 6 hours. 25 compounds exhibited >50% PPI inhibition (Fig. 2C). The other 27

compounds either displayed little inhibition (for 19 compounds), or strong cytotoxicity based on morphological changes (supplementary Fig. S5). We next characterized inhibition kinetics. 19 compounds inhibited the PPI within 2 hours (Fig. 2D). Among these, bruceine D, bruceine A, homoharrington, anisomycin, and gamabufotalin blocked the PPI with $\tau \sim$ 0.5 – 0.7 hour. The remaining compounds showed slower inhibition (supplementary Fig. S6). Lastly, the top 19 compounds had little effect on the SURF control (supplementary Fig. S7).

Antiviral activity against SARS-CoV-2 in cells

We next selected the top performing drugs and natural compounds against the PPI and determined their antiviral activity using SARS-CoV-2 in Vero E6 cells (Fig. 3A). Six of the drugs inhibited SARS-CoV-2 at 5 μM (Fig. 3B). The natural compounds inhibited SARS-CoV-2 replication at 1 or 2 μM (Fig. 3C). Strikingly, gamabufotalin, anisomycin and bruceine A exhibited > 6-log reduction in viral titer at 1 μM. At 0.1 μM concentration, they inhibited SARS-CoV-2 by 10 – 1000-fold (Fig. 3D). Interestingly, brucein D, a structurally related compound to bruceine A, exhibited no inhibition at 0.1 μM (supplementary Fig. S8).

Next, we determined dose-response curve (Fig. 3E). Gamabufotalin had the most potent antiviral activity with an $EC_{50} \sim 0.003$ μM, followed by anisomycin (0.016 μM) and bruceine A (0.054 μM). Interestingly, bruceine A showed 4-fold higher potency than bruceine D. These compounds were largely not cytotoxic in the Vero cells at EC_{50}, with selectivity index (CC_{50}/EC_{50}) > 10. Other natural compounds and FDA-approved drugs showed less potent antiviral activity with EC_{50} at sub-μM (Fig. 3E) or μM range (supplementary Fig. S9). The top 3 inhibitors were further confirmed using antibodies against the nucleocapsid (N) or Spike. At 200 nM, gamabufotalin, anisomycin and bruceine A potently blocked SARS-CoV-2 (Fig. 3F, G). The compounds also blocked SARS-CoV-2 variants Delta and Omicron (Extended Data Fig. 2).

Antiviral activity during SARS-CoV-2 infection

To further understand mode of action, we examined the effects of the natural compounds at three time points before or after SARS-CoV-2 infection (Fig. 4A). For the first condition, we preincubated Vero cells with the inhibitors for 3 hours, followed by addition of SARS-CoV-2 (MOI = 5) for adsorption at 4°C for 1 hour. Then we removed the solution and added fresh medium containing the compounds (Fig. 4A, (i) “−4 hrs”). For the other two conditions, the compounds were added at 1 or 4 hpi (Fig. 4A, (ii) “+1 hr” and (iii) “+4 hrs” samples). The cells were then incubated at 37°C, 16 hours later, the supernatant and cells were collected for the plaque assay and qRT-PCR.

The plaque assay-based measurement of viral particles in the supernatant showed that anisomycin and bruceine A reduced viral titers by 4–5 logs, and gamabufotalin by 2–3 logs (Fig. 4B, (i) “−4 hrs”). For the “+1 hr” samples, anisomycin and bruceine A reduced viral titers by 4 logs, and gamabufotalin by 1–2 logs. The inhibitory effect was further reduced in the “+4 hrs” regimen. Anisomycin and bruceine A showed viral titer reduction by 2 logs, and gamabufotalin by <1 log.

Consistent with the virus production measured in a plaque assay, viral genome copy number measured by qRT-PCR in infected cells showed that for the "−4 hrs" samples, anisomycin, bruceine A and gamabufotalin reduced viral RNA load by 5–6 logs, 4–5 logs, and 2–3 logs, respectively. The inhibitory activity was reduced in the "+1 hr" samples and further reduced in the "+4 hrs" samples (Fig. 4C). These results indicate that the inhibitors act on early stages of the viral infection.

To test if the natural compounds inhibit cellular binding of SARS-CoV-2, we conducted immunofluorescenc-based binding assay. We preincubated the Vero cells with each inhibitor (2 μM) for 3 hours, followed by addition of SARS-CoV-2 (MOI = 100) for adsorption at 4°C for 1 hour (Fig. 4D). Then we removed the solution, washed the cells, PFA-fixed, and stained the samples with the antibodies against the N protein. Immunofluorescence of the N protein was decreased by ~10-fold, suggesting that SARS-CoV-2 viral particle binding to the cells is largely reduced in the presence of inhibitors (Fig. 4D). These results indicate that the inhibitors act by blocking SARS-CoV-2 binding to the host cells.

To further examine whether the inhibitors block PPI of S and ACE2, we utilized the replication-competent recombinant VSVs (rVSVs) encoding the Spike in place of the original G glycoprotein (rVSV-eGFP-SARS-CoV-2) [23]. We examined the inhibitors on the pseudovirus in ACE2-expressing A549 cells (Fig. 4E). Bruceine A, anisomycin and gamabufotalin showed strong inhibition, with an EC_{50} of 0.018, 0.018 and 0.005 μM, respectively. Lastly, we showed that our compounds have no effect on a control virus, a Sindbis virus (supplementary Fig. S10). These results suggest that these compounds exert their activity by blocking PPI of S and ACE2.

Anti-SARS-CoV-2 activity in primary human cells

Next, we determined the antiviral potential of the natural compounds including gamabufotalin, bruceine A and anisomycin in the human primary cells that are relevant to SARS-CoV-2 infection in humans [24]. We used primary human nasal epithelial cells (HNEpC) and primary human bronchial epithelial cells (HBEpC), both of which were cultured in an air-liquid interface. We pre-incubated HNEpC with 2 μM natural compounds for 3 hours before infection (Fig. 5A). We then infected HNE cells with SARS-CoV-2 for 1 hour at 37°C and incubated for 48 hours (both stages in the presence of the 2 μM inhibitors). After viral infection, the cells were fixed and stained with anti-N and anti-S antibodies. Immunofluorescence imaging showed that the natural compounds largely reduced SARS-CoV-2 infection in HNEpCs (Fig. 5B, D). We then conducted similar experiments in HBEpC, with the compounds at 15, 50, and 200 nM, and 1 μM (Fig. 5C, supplementary Fig. S11A). Quantification of the HBEpC imaging data showed that all three compounds reduced the infection even at 15 nM (Fig. 5E, supplementary Fig. S11B). We also confirmed the inhibition effect of gamabufotalin and anisomycin in HNE cells using plaque assays and qRT-PCR (Extended Data Fig. 3). Thus, these inhibitors have potent antiviral activity against SARS-CoV-2 infection in the primary human airway epithelial cells.

We also examined the effects of the natural compounds when given prior to or post-infection of SARS-CoV-2 in HBEpC (Extended Data Fig. 4). First, we preincubated HBEpC with the inhibitors for 3 hours, followed by the addition of SARS-CoV-2 for adsorption for 1

hour. Then we removed the solution and added fresh medium containing the compounds (Extended Data Fig. 4A, (i) "−4 hrs"). For the other two conditions, the compounds were added at 1 or 4 hpi (Extended Data Fig. 4A, (ii) "+1 hr" and (iii) "+4 hrs" samples). The cells were incubated at 37°C for 72 hours and fixed for immunofluorescence staining against SARS-CoV-2 N and S proteins. Our data showed that for all the three compounds, "−4 hrs" samples showed complete inhibition of SARS-CoV-2 infection, "+1 hrs" samples showed ~ 90% inhibition, but "+4 hrs" samples did not show significant inhibition (Extended Data Fig. 4B, C). These results are consistent with those in Vero cells. Our data indicate that these inhibitors act on the early stages of the viral infection in HBEpC. We also examined toxicity of the natural compounds in HBEpC. After incubation with gamabufotalin, bruceine A or anisomycin at 2 μM for 72 hours, no cytotoxicity was observed in HBEpC (supplementary Fig. S12).

Anti-SARS-CoV-2 activity in mouse models of infection

We next determined the antiviral activity of the potent inhibitors, gamabufotalin and bruceine A, in the mouse models of SARS-CoV-2 infection. The K18-hACE2 mice[25] were infected intranasally with SARS-CoV-2 (10^3 PFU per mouse), in the absence (vehicle control, solvent) or presence of the inhibitors. The treatment was repeated on days 1 and 2 (Fig. 6A). We directly examined the effects of bruceine A and gamabufotalin on virus replication. At day 3 post-infection, lungs and brain were harvested for analysis. The two compounds reduced viral titers by 2–3 logs in the lungs (Fig. 6B). Bruceine A treatment reduced SARS-CoV2 titers to undetectable levels in brain tissues (<10 PFU/g; n = 6 animals). Similarly, we were unable to detect virus in the brains of four out of six animals treated with gamabufotalin, and we observed a 1–2 log reduction in viral titers for the remaining two animals. Immunofluorescence imaging analysis revealed similar antiviral activity of bruceine A and gamabufotalin in the lung sections. Immunofluorescence of anti-N and anti-S indicated that the lungs of both bruceine A and gamabufotalin-treated animals showed dramatically fewer N- and S-positive cells than vehicle controls (Fig. 6C, D).

We next examined histopathological changes in the lung by staining the lung sections with hematoxylin and eosin. For the vehicle-treated samples, we detected both alveolar and peribronchial inflammation. The bruceine A-treated lung showed no or little inflammation in the alveolar and peribronchial areas, similar to those from the animals not infected with SARS-CoV-2 (Extended Data Fig. 5 and 6). Gamabufotalin-treated lung also revealed little alveolar and largely reduced peribronchial inflammation.

We also examined whether the inhibitors can block the coronavirus after viral infection in mice. We first infected the wildtype C57BL6 mice with another strain of SARS-CoV-2 (B.1.1.7) via intranasal inoculation without co-application of the inhibitors. Treatments with bruceine A and gamabufotalin were then given twice, at 24 and 48 hpi, via intranasal inoculation elicited protection (Extended Data Fig. 7A). Lungs were harvested for analysis at 72 hpi. Bruceine A and gamabufotalin reduced virus titer in lung by 0.8 and 1 logs, respectively (Extended Data Fig. 7B). Immunofluorescence of anti-N and anti-S showed both drugs largely reduced N- and S-positive cells in lungs (Extended Data Fig. 7C, D).

Histopathological changes in the C57BL6/B.1.1.7 model were mild, but perivascular and alveolar inflammation can still be detected in the vehicle-treated group (Extended Data Fig. 8A). With 5 mice analyzed in each group, significant differences were shown between histopathology score of vehicle-treated group (1.2/16) and bruceine A-treated (0.2/16) or gamabufotalin-treated (0.2/16) groups (Extended Data Fig. 8B). These results suggest that the two natural compounds may provide therapeutic treatment for COVID-19.

DISCUSSION

Several small-molecule inhibitors interfere with aspects of the lifecycle of SARS-CoV-2, including the main protease Mpro [26–29] and the SARS-CoV-2 replicase RdRp[30]. However, no potent small molecules at nanomolar range have been reported to inhibit the interaction of the viral S protein and the host receptor ACE2. In the present study, we designed a brightly fluorescent PPI reporter that visualizes the interaction between spike protein and its receptor. This reporter is fluorogenic and reversible. Its large dynamic range and bright signal enable robust HTS of small-molecule inhibitors in living cells.

Using the fluorogenic PPI reporters, we identified potent inhibitors that block the interaction of the two proteins in living cells at nanomolar concentrations, which were verified to inhibit SARS-CoV-2 infection in Vero cells as well as the primary human airway cells at 15 nM. Additionally, the reversibility of our reporter allowed us to characterize inhibition kinetics of the identified compounds, which, interestingly, is proportional to their efficacy in cells. Our work demonstrates that this innovative reporter and the structure-based engineering strategy can be applied to design reporters for imaging key PPIs that mediate other virus-host interactions in the future, and to screen for small molecule inhibitors, following a similar approach developed here.

Our results suggest that the potent compounds, bruceine A and gamabufotalin, inhibit SARS-CoV-2 infection by blocking the S protein and ACE2-mediated early stages of the viral infection. First, the inhibitors exert their activity on the early stages of the viral infection because the antiviral activities of these inhibitors are significantly reduced when they are added at later stages of viral infection. Second, the SARS-CoV-2 binding assay showed that the inhibitors block the virus binding to the host cells. Lastly, using the pseudovirus, we further determined that the compounds exert their activity by blocking the interaction of the S protein and ACE2, because the pseudovirus only express one of the SARS-CoV-2 proteins, the S protein. Furthermore, these compounds have no activity against SINV that has no spike protein of SARS-CoV-2.

To gain insight into how the compounds inhibit the S-ACE2 interaction, we docked the two compounds into the possible pockets of the S-ACE2 protein complex, and found that both compounds were able to dock into the active site of ACE2 (Extended Data Fig. 9). An ACE2 inhibitor bound to the same site was reported to be effective in blocking the SARS-CoV spike protein-mediated cell fusion [31], which show that the ACE2 inhibitor induces striking conformational changes in the active site that impacts surrounding residues including those in binding to the spike protein. Considering the high sequence similarity between the two spike proteins (~75% homologous) of SARS-CoV and SARS-CoV-2, our compounds may

also inhibit the S-ACE2 interaction as the ACE2 inhibitor, possibly by conformational change of ACE2 that blocks interaction with spike protein.

Considering the SARS-CoV-2 virus constantly changes through mutations, especially in the spike RBD domain, we tested the antiviral effect of bruceine A and gamabufotalin on Delta and Omicron variants. Both compounds maintained similar or slightly weaker inhibition effect on Delta and Omicron infection in Vero cells.

We demonstrate that the two natural compounds (gamabufotalin and bruceine A) exhibit potent antiviral efficacy in vivo when they were administered together with the virus as a prophylactic treatment. We chose these two inhibitors because their analogs showed largely reduced antiviral activity, indicating a structure-activity relationship. For example, cinobufotalin, which is structurally related to gamabufotalin, showed 5-fold lower antiviral activity; Bruceine D has 4-fold lower antiviral activity than bruceine A (Fig. 3E). Both bruceine A and gamabufotalin reduced viral titer in the lung by 2–3 logs on day 3 post-infection using K18-hACE2 mouse models of SARS-CoV-2 infection. These results were verified by immunofluorescence imaging of the lung tissues. Furthermore, bruceine A eliminated the coronavirus in the mouse brain. Gamabufotalin also significantly blocked SARS-CoV-2 replication in the brain. Histopathological analysis of lungs showed a significant reduction of both alveolar and peribronchial inflammation. These findings demonstrate that both inhibitors significantly reduce SARS-CoV-2 replication in the lung and brain, and prevent lung inflammation in the mouse model when the inhibitors were administered together with the virus. On the other hand, when the inhibitors were provided 24 hours post-infection, they show mild activity in blocking viral replication. This is consistent with the results in cultured cells that the inhibitors mainly block early stages of viral infection. Our work suggests that the two compounds may be used as therapeutic treatment for COVID-19 via nasal application of the compounds.

The PPI reporter we have developed in this work visualizes the interaction between spike protein and its receptor ACE2. Our engineering strategy improves the reporter's brightness by ~270-fold. The improved PPI reporter visualizes spike-ACE2 interaction with large dynamic range, which enabled HTS of small molecule inhibitors of this PPI. This reporter strategy will find important applications in the future in studying spike-receptor interactions, and it will also guide future engineering of reporters in imaging spike interaction with other receptors such as neuropillin-1 (NRP1). The spike protein of SARS-CoV-2 has been shown to interact with NRP1 [32], which facilitates infection of SARS-CoV-2 in neurons such as the NRP1-positive olfactory neurons that face the nasal cavity. We further show that the reporter is generalizable because it can be used to visualize the interaction between the spike and NRP1 (Extended Data Fig. 10). This PPI reporter will be valuable in studying spike-NRP1 interaction, as well as identifying small molecule inhibitors by HTS. Therefore, our work provides a general strategy in engineering PPI reporters for imaging interaction between a viral protein and its host cell's receptor, and screening for inhibitors that block viral interaction with host cells. Our PPI reporter, its engineering strategy and the screening approach will be a valuable resource in effectively dealing with future pandemic by SARS-CoV-2 variants and other viruses.

Materials and methods

Plasmid construction

To create the S^{RBD}::ΔACE2 SURF in pcDNA3.1, we used different truncations of the spike (S) protein and ACE2 and fused them to cSURF and nSURF, respectively. The FKBP::Frb SURF was also cloned into pcDNA3.1 using full-length human FKBP CDS and human mTOR Frb domain ($mTOR^{2025-2114}$). pcDNA3.1-S^{RBD}-IFP2 and pcDNA3.1-IFP2-ΔACE2 were created by fusing S^{RBD} or ΔACE2 to IFP2 with a 10 amino acid linker. All constructs were made using standard enzyme digestion and ligation methods.

Cell culture, transfection and live cell imaging

HEK293T cells (ATCC, #3216) were cultured in DMEM (Gibco 11965-092) supplemented with 10% fetal bovine serum (FBS; Gibco 16000044) and 1% penicillin-streptomycin-glutamine (Gibco Invitrogen). Vero-E6 (ATCC, #1586) were maintained in MEM (Gibco Invitrogen) supplemented with 10% FBS and 1% penicillin-streptomycin-glutamine. A549-ACE2 cells were a kind gift from Peter Jackson's lab (Stanford University). All cells were cultured at 37°C in humidified 5% CO_2 incubators.

HEK293T cells were transfected using calcium-phosphate or PEI. All live cell imaging was performed using a Nikon Eclipse Ti inverted microscope equipped with a Yokogawa CSU-W1 confocal scanner unit (Andor) and a CO_2/temperature control unit, using Nikon's NIS-elements software.

For determining inhibition kinetics of the identified drugs, we added each drug (10 μM) to HEK293T cells expressing S^{RBD}::ΔACE2 SURF, performed time-lapse imaging, and analyzed fluorescence changes over time. The inhibition kinetics of each drug was determined from the normalized SURF fluorescence (by the red fluorescence of mCherry) over time. Seven drugs inhibited the PPI within 6 hours. Three of the seven drugs (i.e., mitoxantrone (2 HCl), digoxin, and cinobufotalin) inhibited the PPI relatively fast, with inhibition half-life (τ) within 1.5 hours.

High-throughput screening

A natural compounds library containing 2592 compounds (TargetMol L6000) and an FDA-approved drug library (MedChemExpress HY-L022) containing 1516 compounds were used for HTS. For each screening, HEK293T cells were transfected with the S^{RBD}::ΔACE2 SURF using PEI, and seeded onto 96-well plates at ~5000 cells/well, 6 hours after transfection. A day after seeding, compounds were added to cells at 5 μM final concentration for natural compounds or 10 μM for FDA-approved drugs. After 16 hours of incubation with the compounds, images were taken for each well in the 488 and 561 channels. The cells' total fluorescence was calculated using ImageJ. SURF fluorescence intensity was normalized by mCherry intensity and then compared with value of control wells incubated with DMSO to get fold-change values.

Cytotoxicity assay

Cytotoxicity of the identified compounds on Vero-E6 cells and HBEpC was determined with WST-1 cell proliferation assays (ROCHE, 5015944001). For Vero-E6 cells, about 3000 cells per well were seeded into 96-well plates and cultured for 1 day at 37 °C. 1 μL of each compound at decreasing concentrations was added. After 18 or 72 hours incubation at 37 °C, WST-1 reagents were added to each well and incubated for 1 hour. For HBEpC, cells were cultured on 6.5-mm transwell inserts, compounds were added into the culture medium for 72 hours, then WST-1 reagent was added and incubated for 4 hours. 450- and 650-nm absorbance were measured using an Tecan Infinite M1000 plate reader with the iControl 1.8 software. All experiments were performed in three biological independent repeats.

SARS-CoV-2 strains including Delta and Omicron

A clinical isolate of SARS-CoV-2 (USA-WA1/2020, BEI NR-52281) was propagated in Vero-E6 cells and was used testing drugs in this cell culture. A clinical isolate SARS-CoV-2/human/USA/CA-UCSF-0001C/2020[33] was propagated in A549 cells expressing ACE2 receptor under control of CMV promoter, and was used for mice and primary cells experiments.

Omicron and Delta variants were isolated in Vero-hACE2-TMPRSS2 cells (BEI NR-54970). 200 μL of nasal specimen was added to a well of a 96-well plate and serially diluted 1:1 over five additional wells. 100 μL of freshly trypsinized cells, resuspended in infection media (DMEM with 10% FBS and 200 u/mL penicillin/streptomycin, 5 μg/mL amphotericin B) at 2.5×10^5 cells/mL, were added to each sample dilution. Cells were cultured at 37°C with 5% CO_2 and checked for cytopathic effect from day 2–3. Supernatants were harvested on day 3 after inoculation. 200 μL of P0 was used to infect a confluent T25 flask to generate a P1 culture, harvested after 3 days. Viruses were passaged for 3 times after isolating to get enough higher titer (>10^7 PFU/mL). Viral titers were quantified with plaque assays. All the infections were performed at biosafety level-3 (BSL-3).

Antiviral assay on Vero-E6 cells

To assess the initial antiviral activity and EC_{50} of the drugs, 70% confluent monolayers of Vero-E6 cells (2×10^5 cells/well in 24-well plates) were pretreated with drugs for 3 hours (pretreatment) and then infected with SARS-CoV-2 (MOI=0.5) at 37°C for 1 hour. The virus solution was removed, and cells were washed twice with PBS and added to fresh medium containing drugs/natural compounds or DMSO to continue culture. At 16 hours post-infection, viral titers of the supernatants were determined with plaque assays.

Plaque assay

Confluent monolayers of Vero-E6 cells grown in six-well plates were incubated with the serial dilutions of virus samples (250 μl/well) at 37°C for 1 hour. Next, the cells were overlayed with 1% agarose (Invitrogen) prepared with MEM supplemented with 2% FBS and 1% penicillin-streptomycin-glutamine (100x, Gibco Invitrogen). After 3 days, cells were fixed with 4% formaldehyde for 2 hours, the overlay was discarded, and samples were stained with crystal violet dye.

Adsorption assay

Vero-E6 cell monolayers at 70% confluence grown on coverslips were pre-incubated with natural compounds at 37 °C for 3 hours. Cells were then added with SARS-CoV-2 virus at MOI=100 and immediately placed at 4 °C for 1 hour. The virus suspension was quickly removed, and cells were washed three times with ice-cold PBS. Cells were immediately fixed with 4% PFA for 30 min at room temperature. PFA was further washed with PBS and quenched with 1 M glycine in PBS.

Drug staging experiment

Drugs were added at different stage of the SARS-CoV-2 infection. For "−4 hrs" samples, Vero-E6 cells (~2×10^5 cells/well in 24-well plates) were pretreated with 2 μM compounds for 3 hours (pre-incubation) and infected with SARS-CoV-2 at MOI=5. After 1 hour of incubation at 37 °C, the cells were washed twice with PBS to remove virus and then incubated with fresh medium containing drugs; For "+1 hrs" and "+4 hrs" samples, there was no pre-incubation, and drugs were added 1 hour or 4 hours after infection, respectively. At 16 hours after infection, supernatant was collected for plaque assay and cells were harvested using Trizol reagent (Ambion, USA) for RT-qPCR.

Pseudovirus rVSV-eGFP-SARS-CoV-2

We preincubated ACE2-expressing A549 cells with the compounds for 3 hours, infected the cells with rVSV-eGFP-SARS-CoV-2 (MOI=1) at 37°C for 1 hour, then removed the pseudovirus, added compounds again and cultured the cells for 16 hours. Cells were then imaged, and infection rates were calculated based on percentage of cells with EGFP signal.

SINV-eGFP generation

The eGFP expressing Sindbis virus (SINV-eGFP) was cloned by inserting the eGFP coding sequence into the XbaI site of the double subgenomic Sindbis vector pTE392J (provided by C Rice). Viral genomic RNA was obtained by in vitro transcription using MEGAscript SP6 kit (Invitrogen) and transfected into BHK-21 cells. The initial virus stock was collected from the supernatant of the transfected cells and amplified once by infecting a new culture of BHK-21 cells (Passage 1, P1). Finally, P1 viral stock titration was done by plaque assay in BHK-21 cells. A similar procedure as with the SARS-CoV-2 was followed here to examine effects of the natural compounds in SINV.

Molecular docking

The structure of SARS-CoV-2 spike protein complexed with human ACE2 (PDB ID: 6VW1) was used in the molecular docking calculations. The calculations were performed as previously described [34]. The protonation states of residues in ACE2 active site were visually checked. Atom charges were assigned to the structure using AMBER united atom force field. Energy grids were pre-generated with CHEMGRID for van der Waals potential, with QNIFFT for Poisson-Boltzmann-based electrostatic potential and with SOLVMAP for ligand desolvation penalty. The pre-sampling 3D conformer libraries were generated by ZINC. Compounds were docked against the ACE2 active site using DOCK3.7. The docking

poses were outputted and were examined visually. The figures were generated using UCSF Chimera.

Primary cells infection

Primary human nasal epithelial cells (PromoCell) were pretreated with compounds for 3 hours, infected with virus at MOI=3 and incubated with medium containing 2 μM inhibitors for 48 hours, and fixed with 4% paraformaldehyde in PBS.

Primary human bronchial epithelial cells were cultured on 6.5-mm transwell inserts (Corning, Corning, NY, USA) for 4 weeks at air-liquid interface to obtain a well-differentiated epithelium. Mucus was removed immediately prior to viral infection by washing the apical surface with a prewarmed solution of 10 mM dithiothreitol (DTT; Thermo) in PBS for 10 minutes and then washed twice with PBS without DTT. Cells were inoculated by adding virus to the apical surface at MOI=1. After 1 h, the apical surface was washed twice with PBS and cells were returned to the incubator. Cells were fixed at 72 h post-infection in 4% paraformaldehyde in PBS.

Immunofluorescence

Vero-E6 cells and primary cells were fixed in 4% paraformaldehyde, permeabilized by PBST (PBS with 0.1% Triton X-100), blocked with 2% BSA and 10% goat serum, and incubated with anti-nucleocapsid antibody (1:500 dilution) (Genetex GTX135357) and/or anti-spike antibody (1:600 dilution) (Genetex GTX632604) overnight at 4 °C. After washing three times with PBST, the cells were incubated with goat anti-rabbit IgG H&L (1:800 dilution) (Alexa Fluor® 488) (Abcam, ab150077) or goat anti-mouse IgG H&L (1:800 dilution) (Alexa Fluor® 555) (Abcam, ab150114).

For Vero-E6 and pimary human bronchial epithelial cells, images were acquired using Nikon Eclipse Ti-E Spinning Disk microscope with a 60× NA1.49 Plan-Apo objective. The software was NIS-Element AR 4.20. For primary human nasal epithelial cells, images were acquired on an Everest deconvolution workstation (Intelligent Imaging Innovations) equipped with a Zeiss AxioImager Z1 microscope, CoolSnapHQ cooled CCD camera (Roper Scientific), and a 40× NA1.3 Plan-Apochromat objective lens (Zeiss, 420762-9800). The software used for the acquisition is SlideBook (version 6). All images were processed in ImageJ. Fluorescence signals were calculated by pixel intensity using Analyze Particle function in ImageJ and cell numbers were calculated using Cell Counter plugin in ImageJ.

3 wells of Vero-E6 cells or primary cell cultures were infected for each condition. 10 field views for each well of Vero-E6, 3 field views for each HNE culture and 10 field views for each HBE culture were imaged. In total, 1500 cells were analyzed for each treatment for Vero-E6 or HBEpC; and 500 cells were analyzed for each treatment for HNEpC. The total N- and S-positive cell numbers per 100 cells were used for statistical analysis.

Viral RNA isolation and quantitative PCR

Genomic RNA was extracted from cell pellets using Trizol (Ambion), according to manufacturer instructions. RNA was treated with DNAse I (NEB) and used as template to

reverse-transcribe cDNA by Iscript kit (NEB). qPCR was done using the Luna Universal qPCR Master Mix (NEB) and a CFX connect qPCR Detection System (BioRad). To determine the number of vRNA copies per mL, plasmids containing the nucleocapsid gene of SARS-CoV-2 (cloned from the USA-WA1/2020 isolate) were used as standards and diluted serially 10-fold to determine target copy numbers. Threshold cycle (Ct) values were plotted against the number of target-copies, and the resultant standard curve was used to determine the number of genome equivalents of vRNA in the samples. For cell pellet samples, the vRNA copy number was normalized to the housekeeping gene HRT1. All samples were within the range of linearity of a standard curve, and the primer efficiencies were 100% +/− 5%. The primer sequences targeting nucleocapsid were: 5′-TCCTGGTGATTCTTCTTCAGG-3′ and 5′-TCTGAGAGAGGGTCAAGTGC-3′. HRT1 primers sequences are: 5′-GGTCCTTTTCACCAGCAAGCT-3′ and 5′-TGACACTGGCAAAACAATGCA-3′.

Inhibitor preparation for the in vivo study

Natural products were obtained from MedChemExpress (bruceine-A HY-N0841, gamabufotalin HY-N0883). Natural products were prepared as 100 mg/mL in DMSO, and then each was diluted in solvent [(5% Tween 80, sigma, P4780), 40% PEG300 (MedChemExpress, HY-Y0873, 55% PBS)].

Toxicity test in animals

Natural products were delivered intranasally. Briefly, C57BL6/J mice were anesthetized with isoflurane and inoculated with solvent and compounds with different diluted concentrations in 50 μL (6.5, 3.25, 1.63 mg/kg). Mice were treated every 24 hours for 3 days. No obvious toxicity was observed up to 6.5 mg/kg/mouse by intranasal inoculation.

Antiviral effect test in mouse models

All the antiviral studies were performed in an animal biosafety level 3 facility at the University of California, San Francisco, Department of Immunology and Microbiology. The SARS-CoV-2 experiments were performed in 8–10-week-old K18-hACE2 mice (The Jackson Laboratory, stock number: 034860, B6.Cg-Tg (K18-hACE2) 2Prlmn/J, hemizygous) and C57BL6/J mice (The Jackson Laboratory, Strain #:000664, RRID:IMSR_JAX:000664). Mice were housed and bred in a specific pathogen-free, AAALAC-certified animal facility at UCSF, at ~23°C, 50% humidity under a 12 h light/dark cycle with standard chow diet provided. All procedures were performed in accordance with the guidelines of the Laboratory Animal Center of National Institutes of Health. The Institutional Animal Care and Use Committee of the University of California, San Francisco approved all animal protocols (Approved protocol No. AN178420-02B).

For K18-hACE2 mice, at day 0, we administered solvent, bruceine A, and gamabufotalin and at the same time, 1000 PFU of SARS-CoV-2 in 50 μL (25 μL of virus solution in PBS plus 25 μL of drug solution or solvent) intranasally (I. N.). Then, bruceine A and gamabufotalin were administrated I. N. one time per day for 2 days. Mice were anesthetized with isoflurane before intranasal infection. This experiment was repeated twice independently, a total of eight mice were used in each control or drug-treated group.

For C57BL6/J mice, at day 0, we administered 10^5 PFU of SARS-CoV-2 (B.1.1.7) I. N.. Then, bruceine A and gamabufotalin were administrated I. N. at 24- and 48-hours post infection. A total of five mice were used in each control or drug-treated group.

For virus tissue distribution, at 3 days post-infection (d.p.i.), animals were humanely euthanized. Lungs and brains were harvested. Half of the lungs were fixed in 4% PFA for 72 hours, transferred to 70% ETOH, embedded to paraffin, and processed for the H&E staining and immunofluorescence staining. The other half of lungs and brains were weighted and homogenized in 1 mL of 2% FBS MEM medium with gentle MACS - C tubes (Miltenyi Biotec Catalog# 130-093-237). Samples were centrifuged at 2500 g for 10 min, and the supernatant was transferred to a new set of tubes and then frozen at −80°C for viral titration via plaque assay. Infectious titers were quantified by plaque assay titration using Vero-E6 cells as described above. Unpaired T test was used for tissue distribution analysis.

Mouse lung histological analysis

Tissue samples were embedded into paraffin. Lung tissue blocks were cut into 5-μm sections in the Gladstone pathology and light microscope core facility. Sections were stained with hematoxylin and eosin (H&E), imaged under digital light microscope in UCSF Nikon imaging center and then analyzed by ImageJ. H&E-stained lung sections were examined using a semi quantitative method previously described [35]. The severity of four histopathological parameters (1. perivascular inflammation, 2. bronchial or bronchiolar epithelial degeneration or necrosis, 3. bronchial or bronchiolar inflammation and 4. alveolar inflammation) were defined and a score was assigned for each parameter (“0” - none, “1” - <25%, “2” - 26–50%, “3” - 51–75%, and “4” - >75%). Unpaired T test was used for statistical analysis.

Immunofluorescence examination of lung sections

Deparaffinization, rehydration, and HIER were performed on an a ST4020 small linear stainer (Leica). For deparaffinization, slides were baked at 70°C for 1–1.5 hours, followed by rehydration in descending concentrations of ethanol (100% twice, 95% twice, 80%, 70%, ddH_2O twice; each step for 30 s). Washes were performed using a Leica ST4020 Linear Stainer (Leica Biosystems, Wetzlar, Germany) programmed to three dips per wash for 30 s each. HIER was performed in a Lab VisionTM PT module (Thermo Fisher) using Dako Target Retrieval Solution, pH 9 (S236784–2, DAKO Agilent) at 97°C for 10 min and cooled down to 65°C. After further cooling to room temperature for 30 min, slides were washed for 10 min three times in Tris-buffered saline (TBS), containing 0.1% Tween 20 (Cell Marque; TBST). Sections were then blocked in 5% normal donkey serum in TBST at room temperature for 1 hour, followed by incubation with primary antibodies in the blocking solution. After one overnight incubation of primary antibodies in 4°C, sections were washed three times with TBST and stained with the appropriate secondary antibodies in PBS with 3% bovine serum albumin, 0.4% saponin, and 0.02% sodium azide at room temperature for 1 hour. After this, sections were washed three times with TBST and mounted with ProLong Gold Antifade mounting medium with DAPI (Invitrogen). The primary antibodies and final titrations used were mouse anti-acetylated α-tubulin (1:300; Santa Cruz sc-23950), rabbit anti-SARS-CoV-2 nucleocapsid (1:1000;

GeneTex GTX135361), and mouse anti-SARS-CoV-2 spike (1:600; GeneTex GTX632604). Secondary antibodies include highly cross-adsorbed donkey anti-rabbit Alexa Fluor Plus 647 1:500 (Thermo A32795) and highly cross-adsorbed donkey anti-mouse Alexa Fluor Plus 555 1:500 (Thermo A32773). Fluorescence-immunolabeled images were acquired using a Zeiss AxioImager Z1 microscope or Keyence BZ-X710 fluorescent microscope. Post-imaging processing was performed using FIJI package of ImageJ 1.52t.

Statistics and Reproducibility

All statistics were performed in GraphPad Prism or Microsoft Excel. IC50 or EC50 of drug inhibition, cytotoxicity and antiviral activity was calculated using the non-linear fit function (Variable slope). All SURF reporter test and cell immunofluorescence staining were repeated at least 3 times. Mice lung section immunofluorescence staining was performed in two mice per group and 3 slides per mouse were analyzed. H&E staining was performed in two mice per group for K18-hACE2 mice, and five mice per group for C57BL6 mice, three slides per mouse were prepared. No statistical methods were used to pre-determine sample sizes but our sample sizes are similar to those reported in previous publications [29,35]. Cell cultures and animals were all randomly grouped. Library screening and initial antiviral tests (Figs 2–3) were carried out blindly, labeled with only numbers but not compound names. The following experiments were not blind, since the differences between compounds groups and control groups can be easily observed from imaging data or antiviral tests. No more than two data points, if any, for one drug in the drug library screening were excluded due low imaging quality. One outlier data point in the qRT-PCR assay for anti-Omicron variant test, DMSO group was excluded due to low RNA yield.

Extended Data

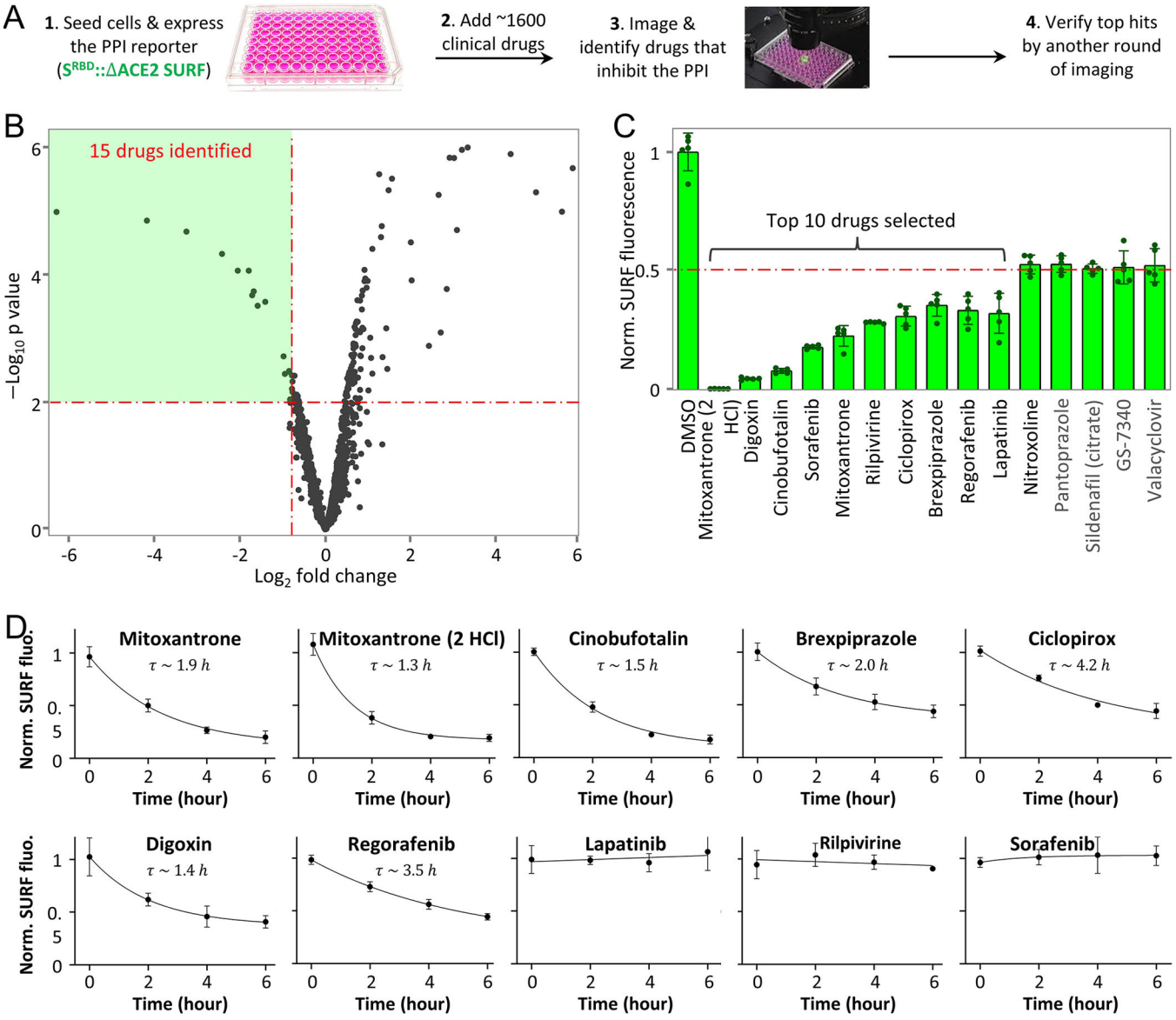

Extended Data Fig. 1. High throughput screening of FDA-approved drugs that inhibits spike and ACE2 interaction using the SURF reporter in living cells.

(**A**) Schematic showing experimental procedure. (**B**) Volcano plot of ~1600 drugs in inhibiting the PPI of spike and ACE2. HEK293T cells were transfected with the SURF reporter. SURF fluorescence was normalized by mCherry. Cells were incubated with compounds at 10 μM concentration for 24 hours before imaging. The dotted horizontal and vertical red lines represent p-value = 0.01 and 40% PPI inhibition, respectively. *P* value, two-sided non-paired t-test between compound- and DMSO-treated groups (n = 5). (**C**) Normalized SURF fluorescence of cells incubated with 15 compounds by a 2nd round of imaging. The dotted red line represents 50% PPI inhibition. Data are mean ± SD (n = 5). (**D**) Inhibition kinetics of the identified drugs against spike and ACE2 interaction. Each clinical drug (10 μM) was added to HEK293T cells expressing the SURF reporter, followed

by time-lapse imaging. Estimated PPI half-time (τ) upon inhibition is shown for each drug. Data are mean ± SD (n = 5).

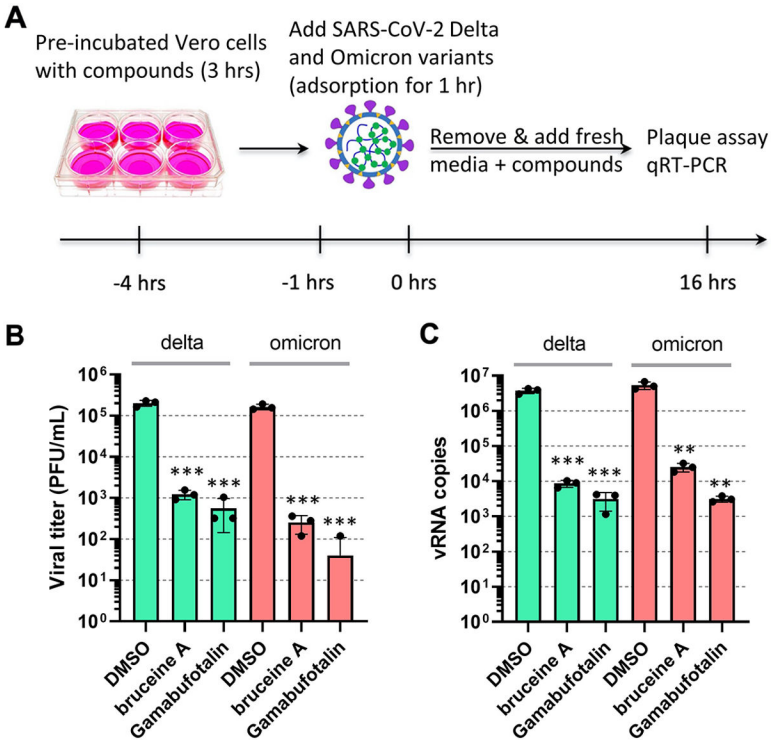

Extended Data Fig. 2. The identified natural compounds inhibit infection of SARS-CoV-2 Delta and Omicron variants.

(**A**) Schematic showing the experimental design, see methods for details.(**B, C**) Quantitative analysis of viral titer by plaque assays (B) and viral RNA genome copies by qRT-PCR (C) on Vero E6 cells treated with drugs at 1 μM. qRT-PCR was performed with primers targeting the nucleocapsid gene (N) of SARS-CoV-2, normalized to internal control HRT1. Green bars indicate results of the Delta variant, red bars indicate results of the Omicron variant. The data are shown as mean ± SD (n =3). *P* value, two-sided non-paired t-test between compound- and DMSO-treated groups. **P < 0.01. ***P < 0.001. Exact *P* values: (B) starting from bruceine A for delta: 0.00048, 0.00048, 0.00034, 0.00034. (C) starting from bruceine A for delta: 0.00052, 0.00052, 0.0022, 0.0021.

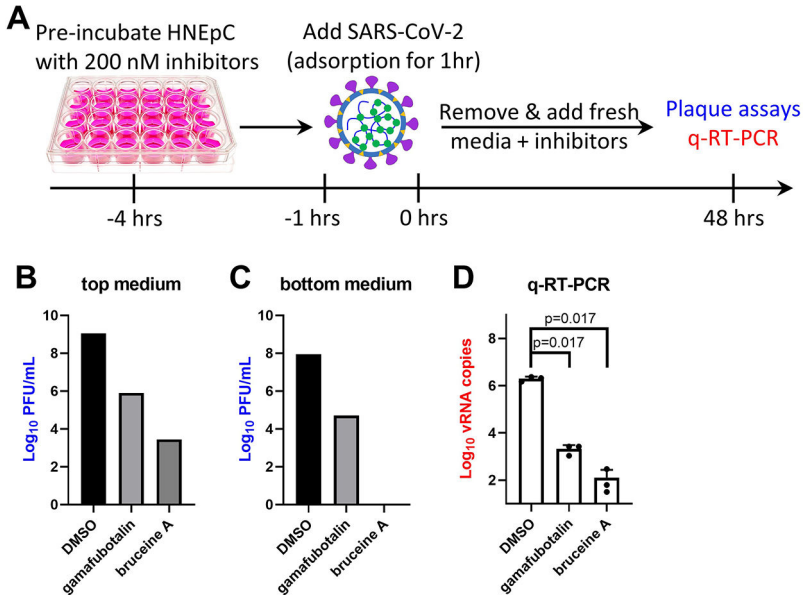

Extended Data Fig. 3. Plaque assays and qRT-PCR confirm gamabufotalin and bruceine A inhibit SARS-CoV-2 infection in primary human nasal epithelial cells.

(A) Experimental procedure. **(B)** Plaque assays using culture medium on top of the transwells. **(C)** Plaque assays using culture medium under the transwells. **(D)** qRT-PCR using HBE cells. The data are shown as mean ± SD (n = 3). *P* value, two-sided non-paired t-test between compound- and DMSO-treated groups.

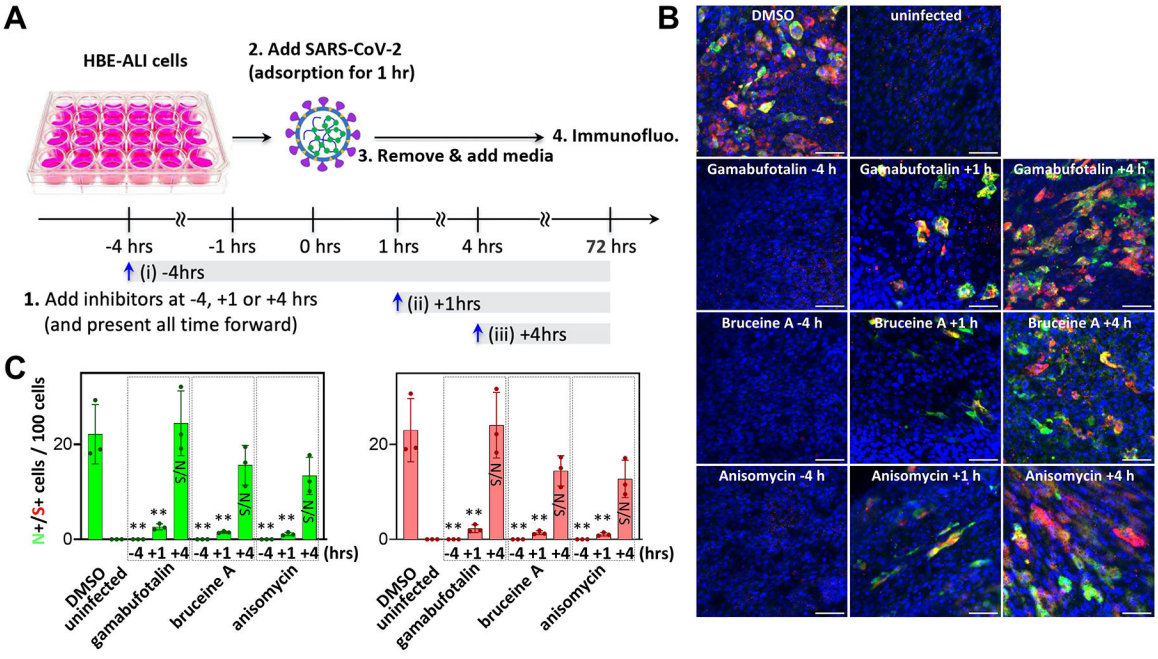

Extended Data Fig. 4. The identified natural compounds inhibit early stages of SARS-CoV-2 infection in primary human bronchial epithelial cells.

(**A**) Experimental procedure. (**B**) Immunofluorescence staining of SARS-CoV-2 in the primary human bronchial (HBEpC) epithelial cells. Gamabufotalin, bruceine A or

anisomycin were added at different timepoints, at 200 nM, MOI = 1. Nucleocapsid is shown in green. Spike is shown in red. Scale bar: 50 μm. (**C**) Quantification of the immunofluorescence images in HBEpC. The data are shown as mean ± SD (n = 3). *P* value, two-sided non-paired t-test between compound- and DMSO-treated groups. **P < 0.01. NS: not significant. Exact *P* values: starting from gamabufotalin anti-N: 0.0036, 0.0057, 0.69, 0.0036, 0.0046, 0.21, 0.0036, 0.0043, 0.11; starting from gamabufotalin anti-S: 0.0039, 0.0059, 0.86, 0.0039, 0.0050, 0.12, 0.0039, 0.0047, 0.083.

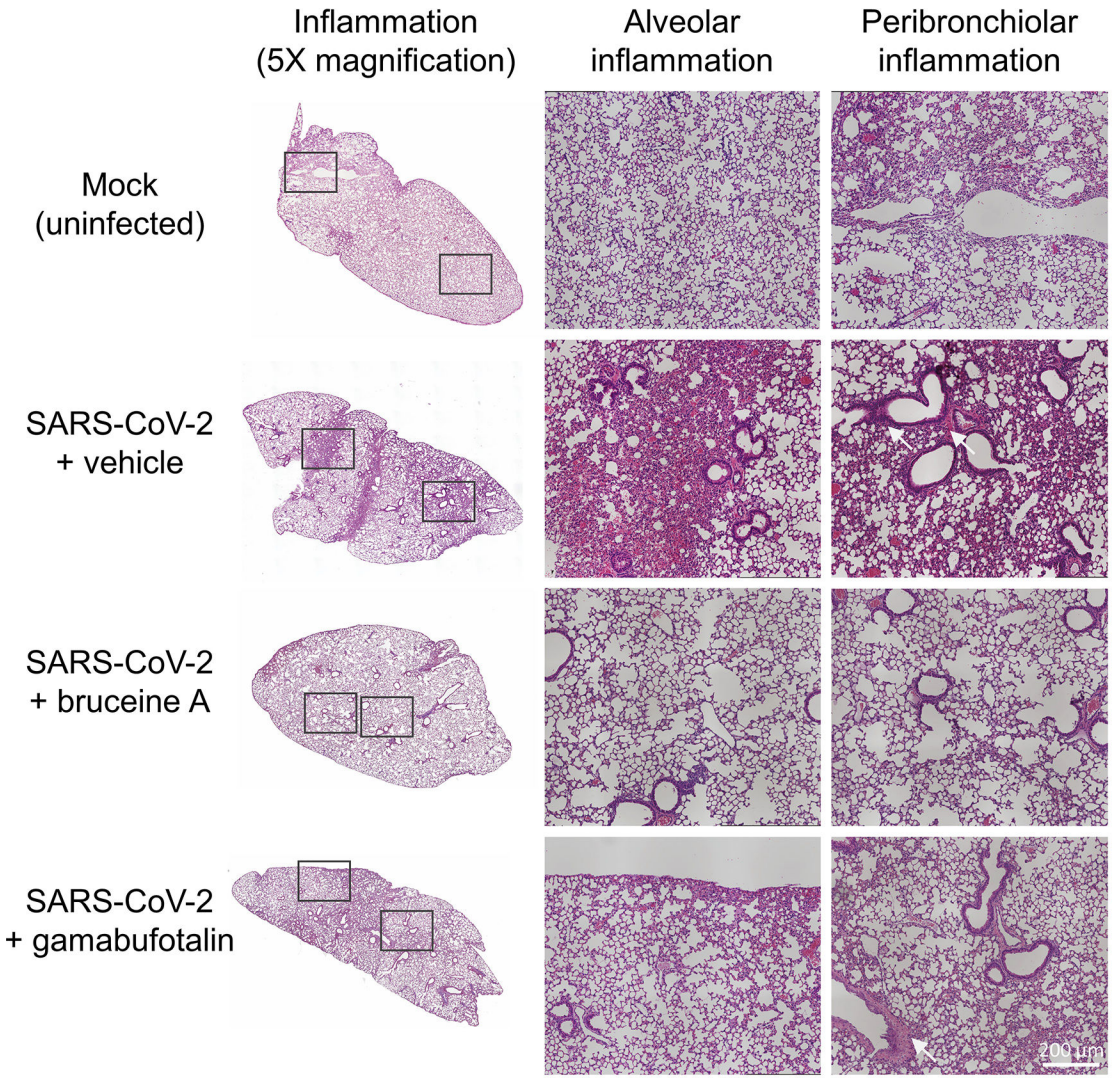

Extended Data Fig. 5. Histopathological analysis of the SARS-CoV-2 infected mice.

H & E analysis of lung sections from the infected mice. K18-hACE2 mice were infected with SARS-CoV-2 (1000 PFU) intranasally with the natural compounds bruceine A, gamabufotalin, or vehicle control (solvent) at day 0. Then the inhibitors were delivered intranasally once per day at day1 and day 2. At day 3 (i.e., 3 days post infection), lungs were harvested and fixed in 4% PFA and embedding into paraffin and cut at 5 μm slides, stained with hematoxylin and eosin (H & E). Black boxes point to regions of the lung anatomy where inflammation was assessed. The magnified images corresponding to the boxed areas

are shown on the right panels. Regions where inflammation was detected are indicated by arrows. Scale bar: 200 μm. The H & E staining was performed in two mice per group and 3 slides per mouse were analyzed.

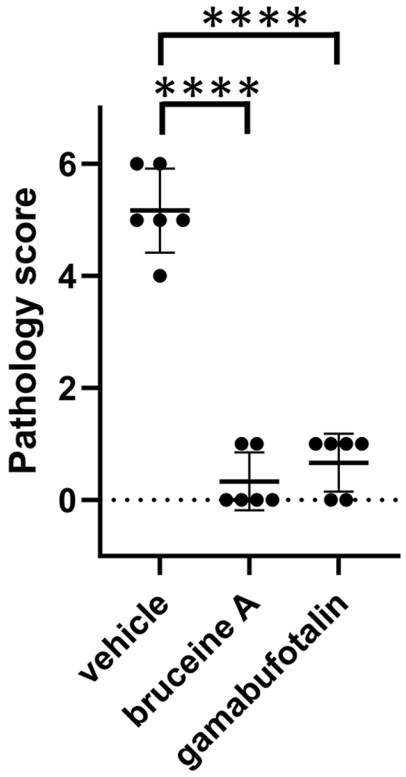

Extended Data Fig. 6. Pathological scores of lung sections.

The semi-quantitative method is described in the methods. For the histology slides, we selected two representative mice out of the 6 mice based on the plaque assay data (Fig. 7B). The dotted black line represents pathology score = 0. Data are mean ± SD. N = 2 independent animals for each treatment group. 3 slides per animal were examined. *P* value, two-sided non-paired t-test between treated and vehicle groups. ****p<0.0001. Exact *P* values: bruceine A 1.4E-07, gamabufotalin 2.8E-07.

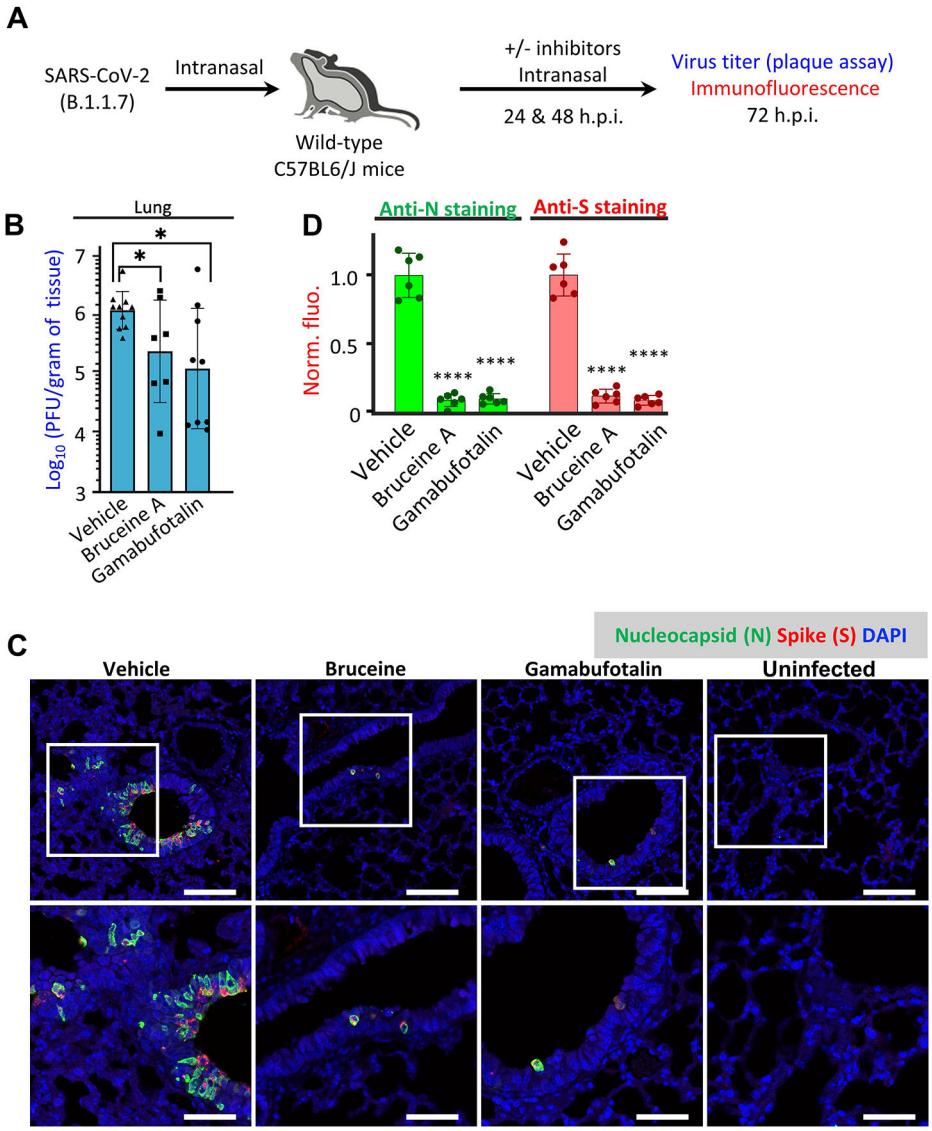

Extended Data Fig. 7. Bruceine A and gamabufotalin exhibit mild activity in inhibiting infection of SARS-CoV-2 B.1.1.7 strain in the C57BL6/J mice.

(**A**) Schematic of the experimental design. C57BL6/J mice were infected by the intranasal route with 10^5 pfu of SARS-CoV-2 (B.1.1.7). Bruceine A and gamabufotalin were used at 3.25 mg/kg by intranasal inoculation at both 24- and 48-hours post-infection. (**B**) Virus loads in Lungs. Lung tissues were collected at 3 days post-infection, homogenized, and supernatants were tittered by plaque assay in Vero-TMPRSS2 cells. Data are shown as mean ± SD. N = 4 independent animals for compound group, and N = 5 independent animals for vehicle group. 2 plaque assays per animal were conducted. Two-tailed Mann-Whitney test was used for statistical analysis. Significance is noted with asterisks as follow: * $p<0.05$. Exact *P* values: bruceine A 0.0412, gamabufotalin 0.0412. (**C**) Immunofluorescence images of the C57BL6/J mice lung tissues. The lung slides were stained with antibodies against nucleocapsid protein (N), spike (S) and DAPI. Immunofluorescence of N, S and DAPI are shown with pseudo-colors green, red and blue, respectively. Lower panels correspond

to the boxed areas of the upper panels. Scale bar, 100 μm (upper panels); 50 μm (lower panels). (**D**) Quantification of the immunofluorescence. Data are shown as mean ± SD. N = 2 independent animals for each treatment group. 3 slides per animal were examined. P value, two-sided non-paired t-test between compound- and DMSO-treated groups. ****P < 0.0001. Exact *P* values: anti-N: bruceine A 1.1E-07, gamabufotalin 1.0E-07; anti-S: bruceine A 1.1E-07, gamabufotalin 5.8E-08.

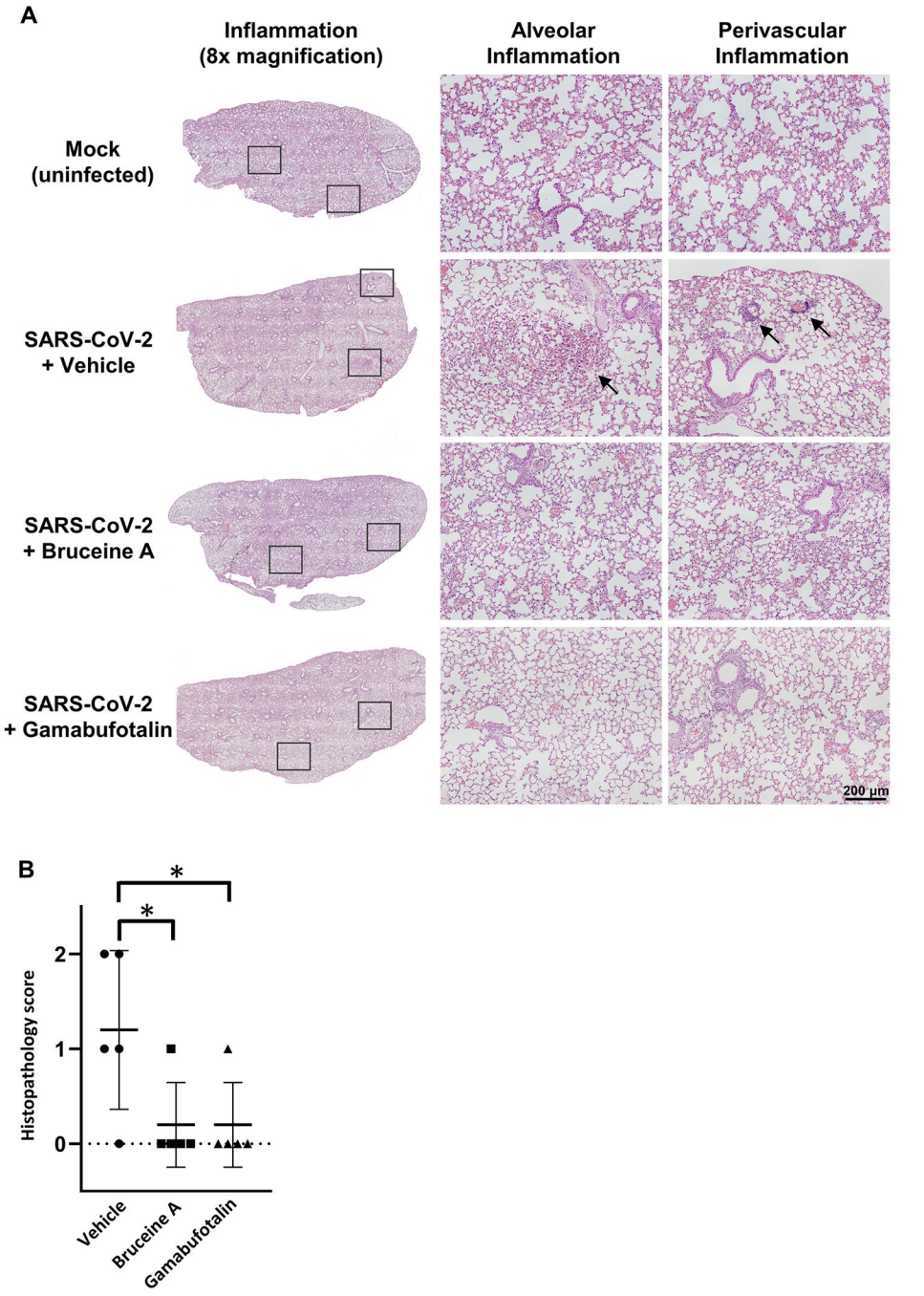

Extended Data Fig. 8. Histopathological analysis of the infection of SARS-CoV-2 B.1.1.7 strain in C57BL6 mice.

(**A**) H & E staining of lung sections from the infected mice. C57BL6 mice were infected by the intranasal route with 10^5 pfu of SARS-CoV-2 (B.1.1.7). Bruceine A and gamabufotalin were used as 3.25 mg/kg by intranasal inoculation at both 24- and 48-hours post-infection. At day 3 (i.e., 3 days post infection), lungs were harvested and fixed in 4% PFA and embedding into paraffin and cut at 5 μm slides, stained with hematoxylin and eosin (H & E). Black boxes point to regions of the lung anatomy where inflammation was assessed. The magnified images corresponding to the boxed areas are shown on the right panels. Regions where inflammation was detected are indicated by arrows. Scale bar: 200 μm. (**B**) Pathological scores of lung sections. Five mice in each group were analyzed using a semi-quantitative method described in the methods. The dotted black line represents pathology score = 0. Data are shown as mean ± SD. *P* value, two-sided non-paired t-test between treated and vehicle groups. *P < 0.05. Exact *P* values: bruceine A 0.046, gamabufotalin 0.046.

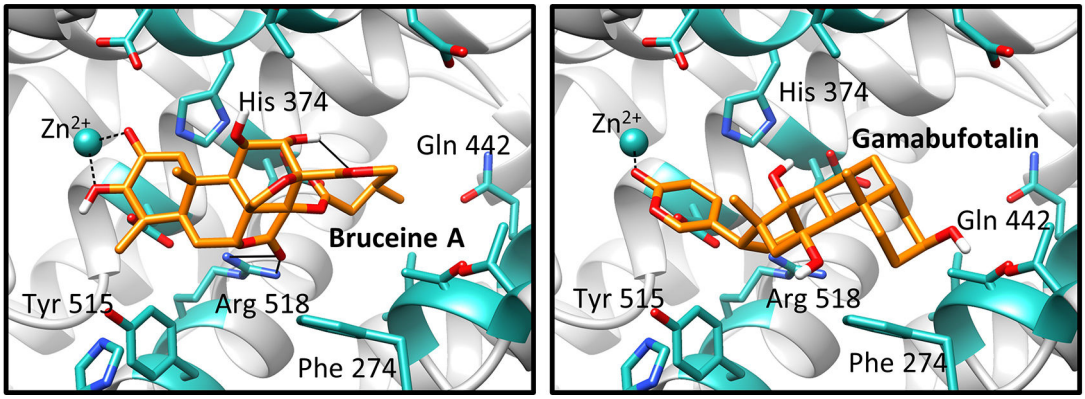

Extended Data Fig. 9. Models of binding poses of Bruceine A (left) and Gamabufotalin right) in the ACE2 active site.

The compounds are colored by orange. The residues in ACE2 active pocket are colored by light green. The hydrogen bonds are illustrated with black solid lines. The co-ordinations with zinc ion are shown with black dashed lines. For both bruceine A and gamabufotalin, the poses with highest possibility were generated via docking the compounds into the active site of ACE2. Bruceine A forms good polar and non-polar interactions with protein residues. The carbonyl and hydroxyl groups coordinate with the zinc ion in the ACE2 protein and another carbonyl group forms decent hydrogen bonds with Arg 518. Bruceine A also has good hydrophobic contacts with Tyr 515, Phe 274, Ile 446 and Thr 371. Gamabufotalin also coordinates with the zinc ion via its carbonyl group and shows hydrophobic contacts with ACE2. These models show possible binding poses of bruceine A and gamabufotalin in human ACE2 protein.

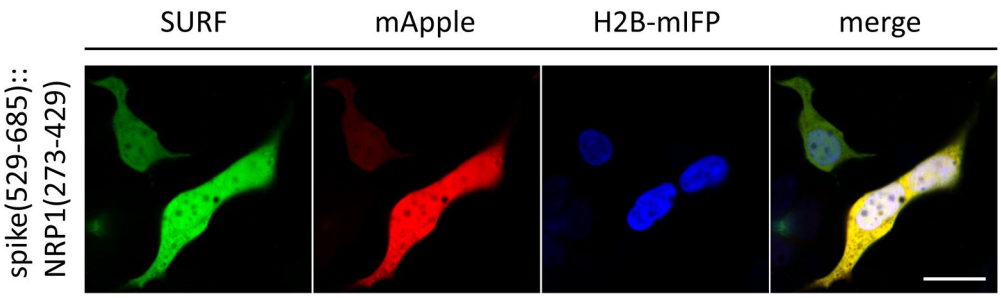

Extended Data Fig. 10. The PPI reporter SURF can be used to image interaction between Spike and NRP1.

Spike(529-685aa) and NRP1(273-429aa) are fused to each part of SURF. The SURF reporter was transiently co-transfected into HEK293T with mApple_T2A_H2B-mIFP. Green: SURF fluorescence. Red: mCherry fluorescence. Blue: mIFP fluorescence. Scale bar: 20 μm. The experiments were repeated for three times independently with similar results.

Supplementary Material

Refer to Web version on PubMed Central for supplementary material.

Acknowledgments:

We would like to thank Drs. David Gordon and Nevan Krogan for sharing the cDNA of spike protein of SARS-CoV-2. Dr. Sean P.J. Whelan for sharing the rVSV-eGFP-SARS-CoV-2 pseudo virus. Drs. Soumya G. Remesh, Kevin Leung and Jim Wells for helps on the PPI assay. Dr. Lauren Rodriguez for helps on the plaque assay for HBEpC.

Funding:

This work was supported by the UCSF Program for Breakthrough Biomedical Research (funded in part by the Sandler Foundation) and NIH (R35GM131766) to X.S., NIH (R01 AI36178, AI40085, P01 AI091575), the Bill and Melinda Gates Foundation and the DARPA Intercept program (Contract No. HR0011-17-2-0027) to R.A, NIH (R35 HL145235, U19 AI077439) to D.J.E.

Data availability:

All data are available within the paper and its supplementary information. The complete screening results and raw data for mouse experiments can be found in the source data section.

References

1. Taylor PC et al. Neutralizing monoclonal antibodies for treatment of COVID-19. Nat Rev Immunol 1–12 (2021). [PubMed: 33303954]
2. Dai L & Gao GF Viral targets for vaccines against COVID-19. Nat Rev Immunol 1–10 (2021). [PubMed: 33303954]
3. Annavajhala MK et al. Emergence and expansion of SARS-CoV-2 B.1.526 after identification in New York. Nature 1–17 (2021).
4. Lan J et al. Structure of the SARS-CoV-2 spike receptor-binding domain bound to the ACE2 receptor. Nature 1–19 (2020).
5. Wang Q et al. Structural and Functional Basis of SARS-CoV-2 Entry by Using Human ACE2. Cell 1–21 (2020).

6. Wrapp D et al. Cryo-EM structure of the 2019-nCoV spike in the prefusion conformation. Science 367, 1260–1263 (2020). [PubMed: 32075877]
7. Yan R et al. Structural basis for the recognition of the SARS-CoV-2 by full-length human ACE2. Science eabb2762–10 (2020).
8. Glebov OO Understanding SARS-CoV-2 endocytosis for COVID-19 drug repurposing. FEBS J 92, 207–8 (2020).
9. Shang J et al. Cell entry mechanisms of SARS-CoV-2. Proceedings of the National Academy of Sciences 117, 11727–11734 (2020).
10. Cao L et al. De novo design of picomolar SARS-CoV-2 miniprotein inhibitors. Science eabd9909–11 (2020).
11. Chan KK et al. Engineering human ACE2 to optimize binding to the spike protein of SARS coronavirus 2. Science 369, 1261–1265 (2020). [PubMed: 32753553]
12. Yuan M et al. A highly conserved cryptic epitope in the receptor-binding domains of SARS-CoV-2 and SARS-CoV. Science eabb7269–10 (2020).
13. Zhang G, Pomplun S, Loftis AR, Loas A & Pentelute BL The first-in-class peptide binder to the SARS-CoV-2 spike protein. bioRxiv 1–15 (2020).
14. Kumagai A et al. A Bilirubin-Inducible Fluorescent Protein from Eel Muscle. Cell 153, 1602–1611 (2013). [PubMed: 23768684]
15. To T-L, Zhang Q & Shu X Structure-guided design of a reversible fluorogenic reporter of protein-protein interactions. Protein Science 25, 748–753 (2016). [PubMed: 26690964]
16. Szymczak AL et al. Correction of multi-gene deficiency in vivo using a single 'self-cleaving' 2A peptide-based retroviral vector. Nat Biotechnol 22, 589–594 (2004). [PubMed: 15064769]
17. Campbell RE et al. A monomeric red fluorescent protein. Proc Natl Acad Sci USA 99, 7877–7882 (2002). [PubMed: 12060735]
18. Shaner NC et al. Improved monomeric red, orange and yellow fluorescent proteins derived from Discosoma sp. red fluorescent protein. Nat Biotechnol 22, 1567–1572 (2004). [PubMed: 15558047]
19. Shu X, Shaner NC, Yarbrough CA, Tsien RY & Remington SJ Novel chromophores and buried charges control color in mFruits. Biochemistry 45, 9639–9647 (2006). [PubMed: 16893165]
20. Shu X et al. Mammalian expression of infrared fluorescent proteins engineered from a bacterial phytochrome. Science 324, 804–807 (2009). [PubMed: 19423828]
21. Yu D et al. An improved monomeric infrared fluorescent protein for neuronal and tumour brain imaging. Nature Communications 5, (2014).
22. Zhang J, Chung T & Oldenburg K A Simple Statistical Parameter for Use in Evaluation and Validation of High Throughput Screening Assays. Journal of Biomolecular Screening 4, 67–73 (1999). [PubMed: 10838414]
23. Case JB et al. Neutralizing Antibody and Soluble ACE2 Inhibition of a Replication-Competent VSV-SARS-CoV-2 and a Clinical Isolate of SARS-CoV-2. Cell Host Microbe 28, 475–485.e5 (2020). [PubMed: 32735849]
24. Ryu G & Shin H-W SARS-CoV-2 Infection of Airway Epithelial Cells. Immune Netw 21, e3 (2021). [PubMed: 33728096]
25. Winkler ES et al. SARS-CoV-2 infection of human ACE2-transgenic mice causes severe lung inflammation and impaired function. Nat Immunol 1–21 (2020). [PubMed: 31831887]
26. Dai W et al. Structure-based design of antiviral drug candidates targeting the SARS-CoV-2 main protease. Science eabb4489–10 (2020). [PubMed: 32321856]
27. Jin Z et al. Structure of Mpro from COVID-19 virus and discovery of its inhibitors. Nature 1–28 (2020).
28. Zhang L et al. Crystal structure of SARS-CoV-2 main protease provides a basis for design of improved α-ketoamide inhibitors. Science 368, 409–412 (2020). [PubMed: 32198291]
29. Li X et al. Ethacridine inhibits SARS-CoV-2 by inactivating viral particles. PLoS Pathog 17, e1009898 (2021). [PubMed: 34478458]
30. Yin W et al. Structural basis for inhibition of the RNA-dependent RNA polymerase from SARS-CoV-2 by remdesivir. Science eabc1560–10 (2020).

31. Huentelman MJ et al. Structure-based discovery of a novel angiotensin-converting enzyme 2 inhibitor. Hypertension 44, 903–906 (2004). [PubMed: 15492138]
32. Daly JL et al. Neuropilin-1 is a host factor for SARS-CoV-2 infection. Science 370, 861–865 (2020). [PubMed: 33082294]
33. Samuel RM et al. Androgen Signaling Regulates SARS-CoV-2 Receptor Levels and Is Associated with Severe COVID-19 Symptoms in Men. Cell Stem Cell 27, 876–889.e12 (2020). [PubMed: 33232663]
34. Bender BJ et al. A practical guide to large-scale docking. Nat Protoc 16, 4799–4832 (2021). [PubMed: 34561691]
35. White KM et al. Plitidepsin has potent preclinical efficacy against SARS-CoV-2 by targeting the host protein eEF1A. Science 371, 926–931 (2021). [PubMed: 33495306]

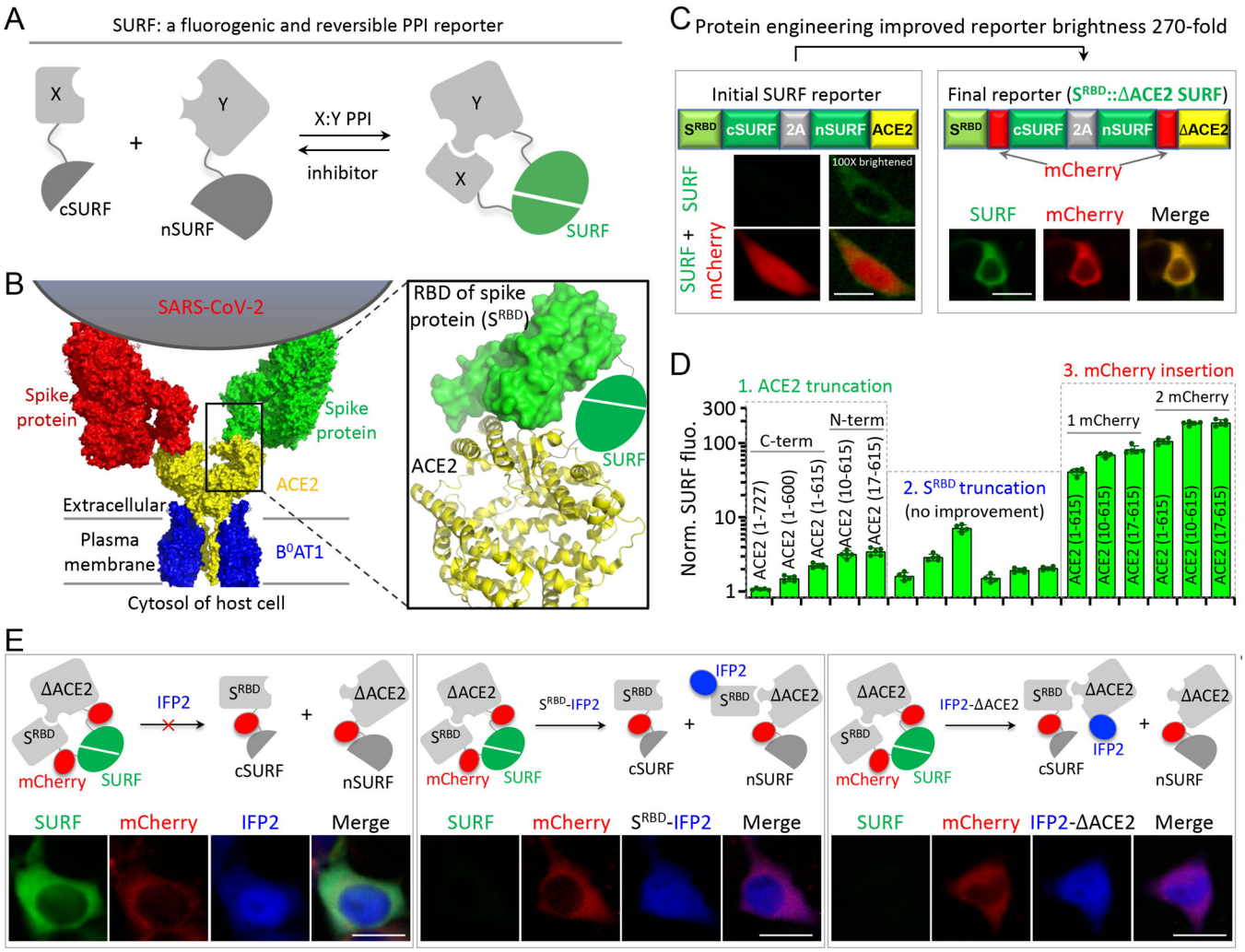

Fig. 1. Engineering fluorogenic reporters for imaging spike and ACE2 interaction in cells.

(**A**) Schematic of the PPI reporter SURF that is based on a split fluorescent protein. X and Y are two proteins of interest. (**B**) Schematic of structure-based design of an initial SURF reporter for imaging spike and ACE2 interaction. (**C**, **D**) Fluorescence images (C) and quantification (D) of the initial and improved SURF reporters in imaging spike and ACE2 interaction. The SURF brightness was improved by 270-fold via protein engineering by ACE2 truncation and mCherry insertion. S^{RBD} (residues 319–541) truncations refer to (left to right): S^{RBD} (333–541) with ACE2(1–615; 10–615; 17–615), S^{RBD} (333–518) with ACE2 (1–615; 10–615; 17–615). Data are mean ± SD (n = 5). (**E**) The final SURF reporter, S^{RBD}::ΔACE2 SURF, is bright and reversible. ΔACE2: truncated ACE2 (residues 17–615). IFP2: a near-infrared fluorescent protein. The experiments were repeated for three times independently with similar results. Scale bar: 20 μm (C, D).

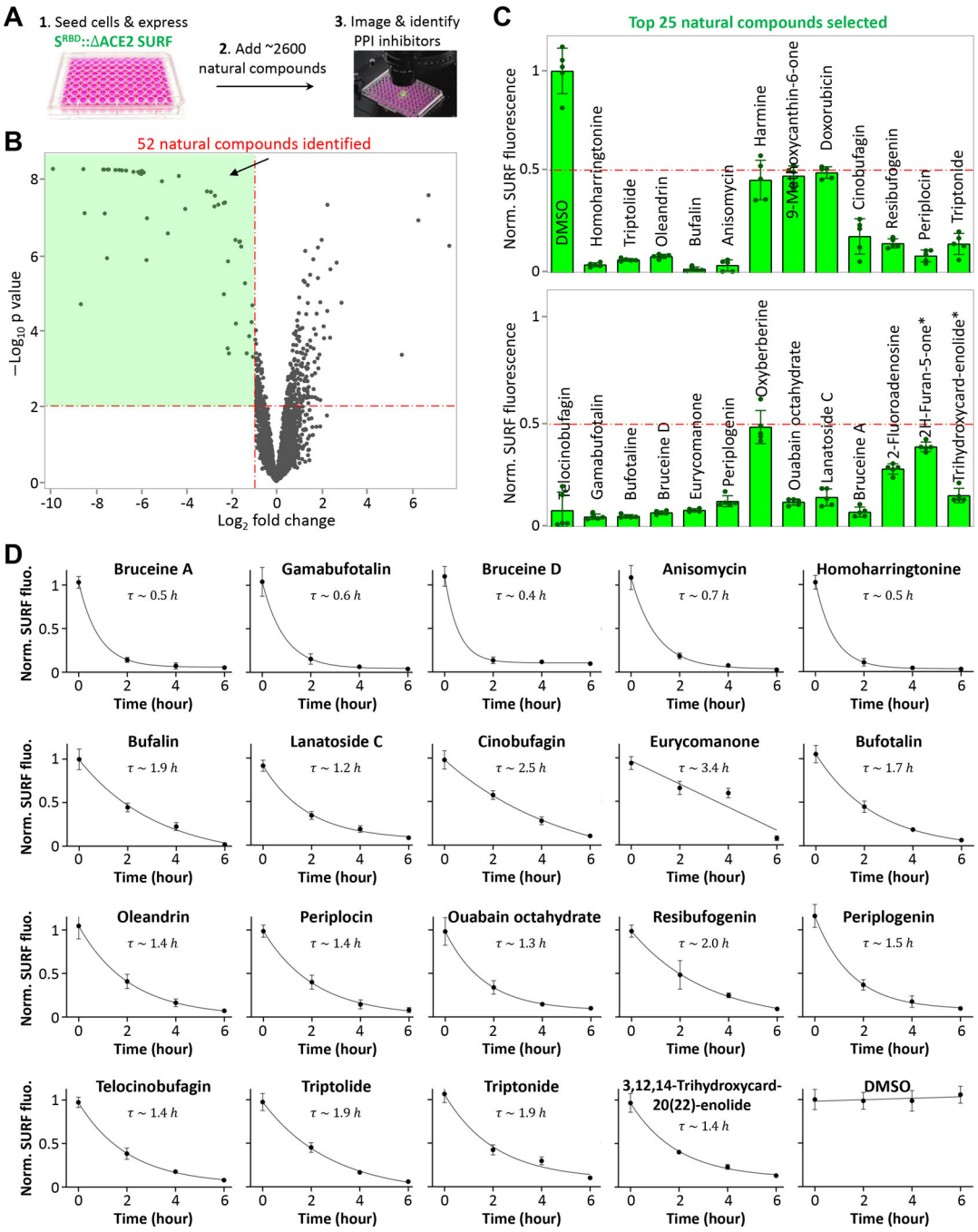

Fig. 2. High throughput screening of natural compounds that inhibit spike and ACE2 interaction.

(**A**)Schematic showing experimental procedure. (**B**) Volcano plot of ~2600 natural compounds in inhibiting PPI of spike and ACE2. HEK293T cells were transfected with SURF reporter. SURF fluorescence was normalized by mCherry. Cells were incubated with each compound at 10 μM for 24 hours before imaging. The dotted horizontal and vertical red lines represent p-value = 0.01 and 50% PPI inhibition, respectively. *P* value, two-sided non-paired t-test between compound- and DMSO-treated groups (n = 5). (**C**) Normalized

SURF fluorescence of cells pre-incubated with 25 compounds (10 μM) for 6 hours. The dotted red line represents 50% PPI inhibition. Data are mean ± SD (n = 5). (**D**) Inhibition kinetics of the identified natural compounds against spike and ACE2 interaction. Each compound (10 μM) was added to HEK293T cells expressing the SURF reporter, followed by time-lapse imaging. Estimated PPI half-life (τ) upon inhibition is shown for each compound. Data are mean ± SD (n = 5).

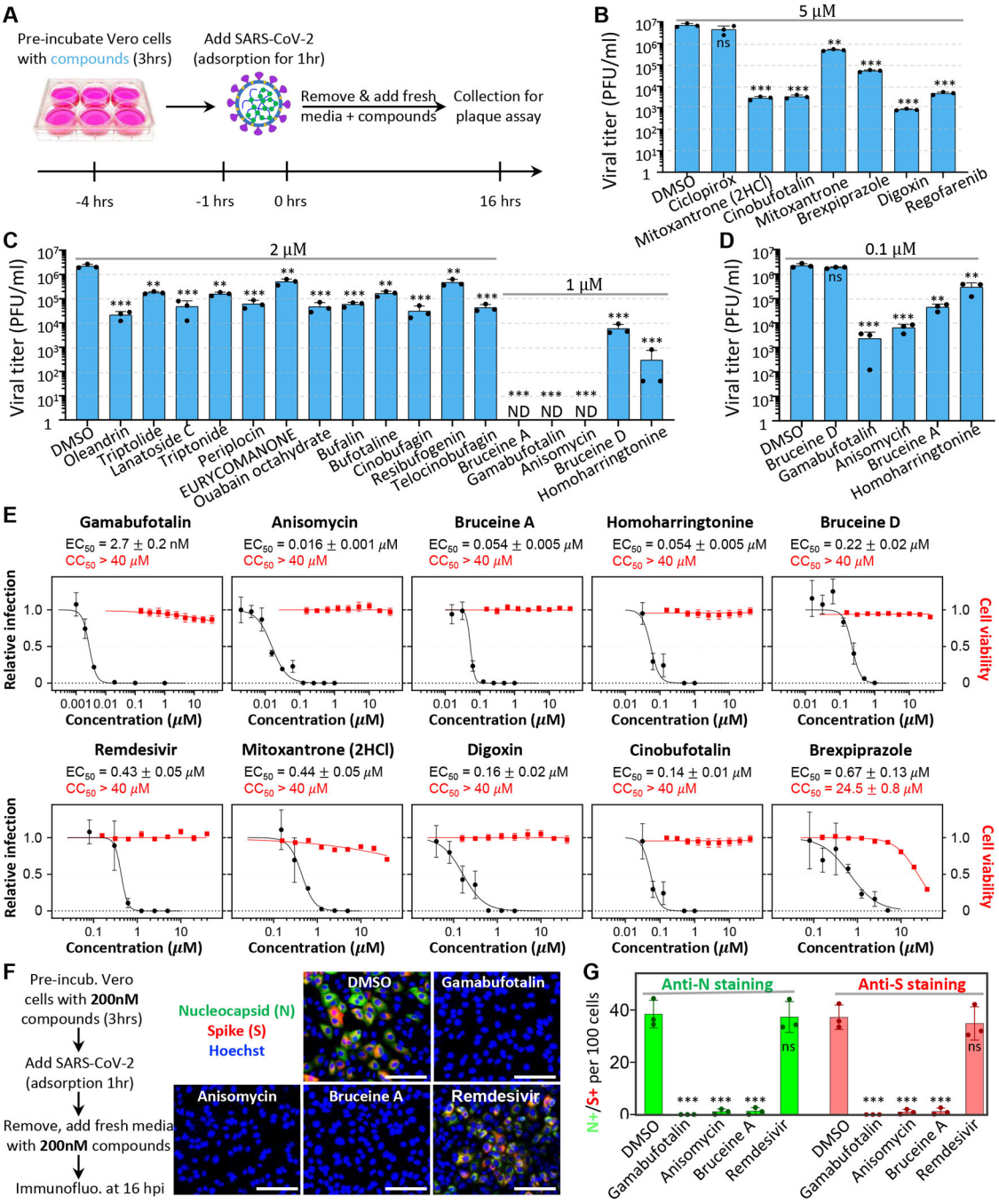

Fig. 3. Antiviral activities of the identified natural compounds and drugs against SARS-CoV-2.

(**A**) Schematic showing the experimental design, see methods for details. (**B - D**) Quantitative analysis of viral titer from plaque assays on Vero E6 cells treated with drugs at 5μM (**B**), or natural compounds at 2 or 1 μM (**C**), or at 0.1 μM (**D**). MOI = 0.5. Data are mean + SD (n = 3). ND: not detectable. *P* value, two-sided non-paired t-test between compound- and DMSO-treated groups. * $p < 0.05$. ** $p < 0.01$. *** $p < 0.001$. Exact *P* values: (B) starting from ciclopirox: 0.14, 0.00096, 0.00096, 0.0013, 0.00099, 0.00096, 0.00096. (C) starting from oleandrin: 0.00083, 0.0011, 0.00088, 0.0011, 0.00090, 0.0026,

0.00087, 0.00089, 0.0011, 0.00085, 0.0025, 0.00087, 0.00080, 0.00080, 0.00080, 0.00081, 0.00080. (D) starting from bruceine D: 0.22, 0.00093, 0.00093, 0.0010, 0.0020. (**E**) Dose-response and cell-toxicity curve of each compound against SARS-CoV-2 by plaque assays (MOI = 0.5). The percentage of relative infection was determined by the ratio of infection rate of SARS-CoV-2 treated with each compound divided by that of DMSO control.EC50 and CC50 are represented as mean ± SD (n = 3). (**F, G**) Immunofluorescence staining (F) of SARS-CoV-2 nucleocapsid and spike protein in Vero E6 cells and quantification (G) of number of stained cells at 16 hpi (MOI = 0.5), treated with 200 nM anisomycin, bruceine A, gamabufotalin or remdesivir. Scale bar, 100 μm (F). Data are shown as mean ± SD (n = 3). *P* value, two-sided non-paired t-test between compound- and DMSO-treated groups. ***P < 0.001. Exact *P* values: starting from gamabufotalin anti-N: 0.00023, 0.00028, 0.00029, 0.82; starting from gamabufotalin anti-S: 0.00016, 0.00019, 0.00021, 0.63.

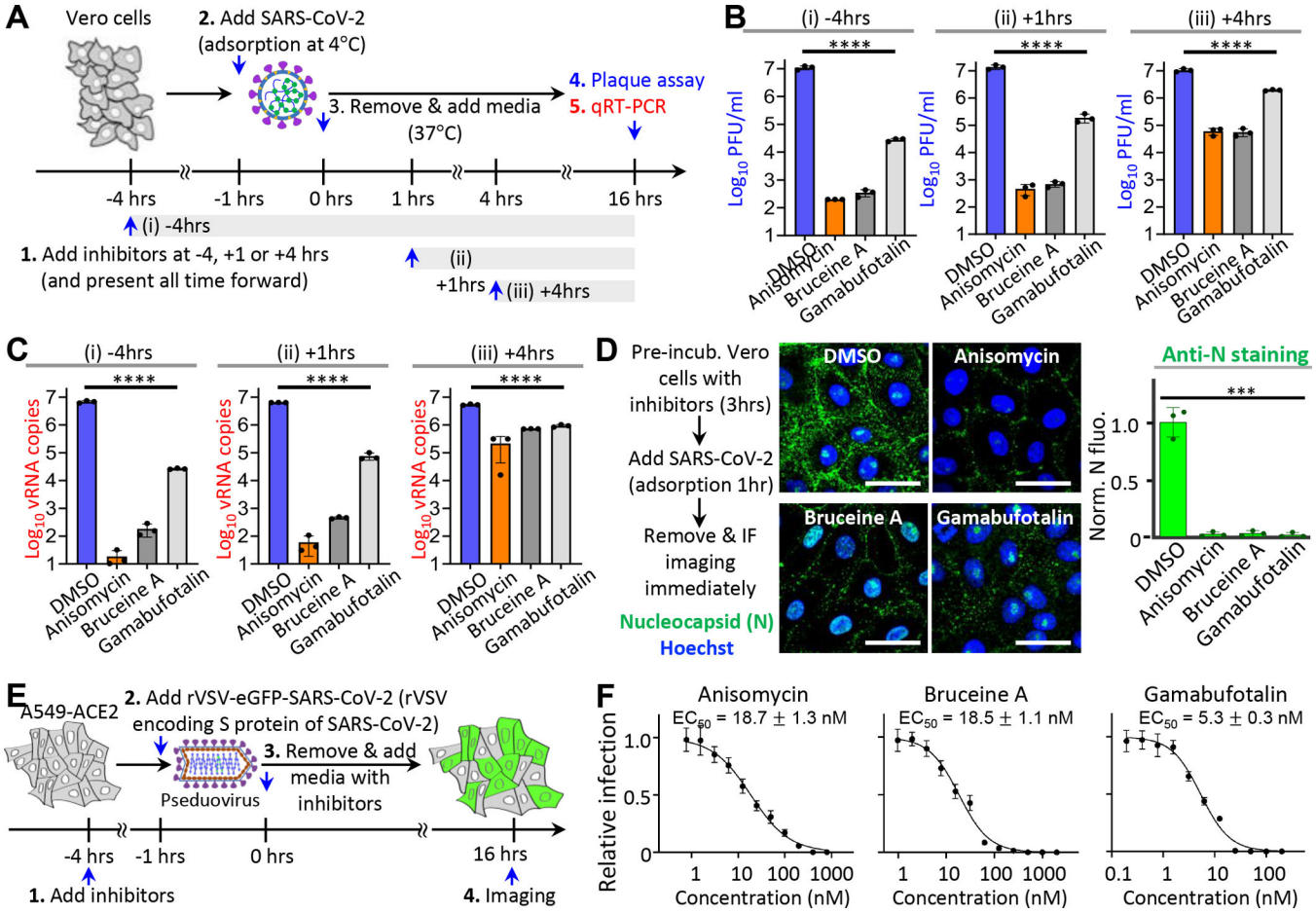

Fig. 4. The identified natural compounds inhibit early stages of SARS-CoV-2 infection.

(**A**) Schematic of the staging experiment. SARS-CoV-2 (MOI = 5) was added to Vero E6cells. The natural compounds (1 μM) were added at various time points as indicated. The samples were characterized by plaque assay (B) and qRT-PCR (C). (**B**) Plaque assay. (**C**) qRT-PCR. Total RNAs were extracted from the Vero cells with Trizol reagents. Viral RNA genomes were measured by qRT-PCR with primers targeting the nucleocapsid gene (N) of SARS-CoV-2, normalized to internal control HRT1. (**D**) SARS-CoV-2 binding assay with immunofluorescence staining. The Vero cells were preincubated with the natural compounds (2 μM), followed by addition of SARS-CoV-2 (MOI = 100) for adsorption at 4 °C for 1 h. Left, experimental procedures. Middle, immunofluorescence images. Right, quantification of immunofluorescence against N protein. All the data (B – D) are shown as mean ± SD (n = 3). *P* value, two-sided non-paired t-test between compound- and DMSO-treated groups. *p<0.05 as significant. **p <0.01, ***p<0.001, ****p<0.0001. Exact *P* values: (B-C) all < 0.0001. (D) starting from anisomycin: 0.00020, 0.00021, 0.00020. Final concentration of the natural compounds was 2 μ M for the above experiments. Scale bar, 40 μm (D). (**E**) Schematic of the rVSV-eGFP-SARS-CoV-2 pseudovirus infection assay. The rVSV-eGFP-SARS-CoV-2 pseudovirus are replication-competent recombinant VSVs (rVSVs) encoding the spike protein of SARS-CoV-2 in place of the original G glycoprotein. A549 cells stably expressing hACE2 were preincubated with the natural compounds for

3 hours, followed by incubation with rVSV-eGFP-SARS-CoV-2 (MOI = 1) at 37 °C for 1 h, then washed with fresh media containing the compounds. EGFP fluorescence of the cells was imaged at 16 hpi. (**F**) Dose-response curves of the inhibitors against rVSV-eGFP-SARS-CoV-2 pseudovirus infection assay. The relative infection was calculated based on eGFP fluorescence. Data are mean ± SD (n = 3).

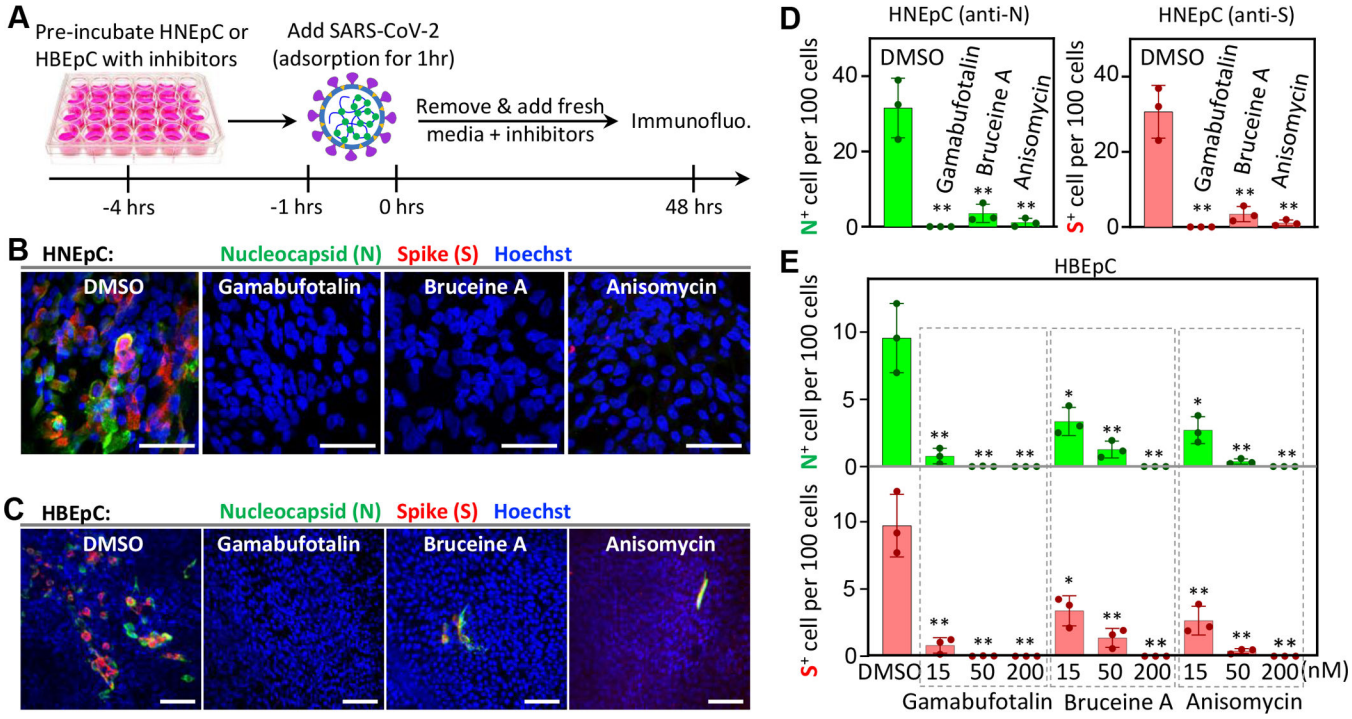

Fig. 5. Inhibition of SARS-CoV-2 in the primary human nasal and bronchial epithelial cells by the identified natural compounds.

(**A**) Experimental procedure. (**B, C**) Immunofluorescence staining of SARS-CoV-2 in the primary human nasal (HNEpC, B) and bronchial (HBEpC, C) epithelial cells, treated with gamabufotalin, bruceine A or anisomycin at 2 μM (B) or 50 nM (C). MOI=3 for HNEpC, MOI=1 for HBEpC. Scale bar, 50 μm (B) and 100 μm (C). (**D, E**) Quantification of nucleocapsid-positive (N^+) or spike-positive (S^+) cells. HNEpC (D) and HBEpC (E) were immunostained with N or S. The number of N^+ or S^+ cells per 100 cells were quantified. The dotted gray rectangles represent samples treated with the same compound at different concentrations. The data are shown as mean ± SD (n =3). *P* value, two-sided non-paired t-test between compound- and DMSO-treated groups. *P < 0.05, **P < 0.01. Exact *P* values: (D) starting from gamabufotalin anti-N: 0.0023, 0.0042, 0.0027; starting from gamabufotalin anti-S: 0.0016, 0.0030, 0.0019. (E) starting from gamabufotalin anti-N: 0.0045, 0.0030, 0.0030, 0.018, 0.0056, 0.0030, 0.013, 0.0035, 0.0030; starting from gamabufotalin anti-S: 0.0030, 0.0020, 0.0020, 0.013, 0.0040, 0.0020, 0.0088, 0.0023, 0.0019.

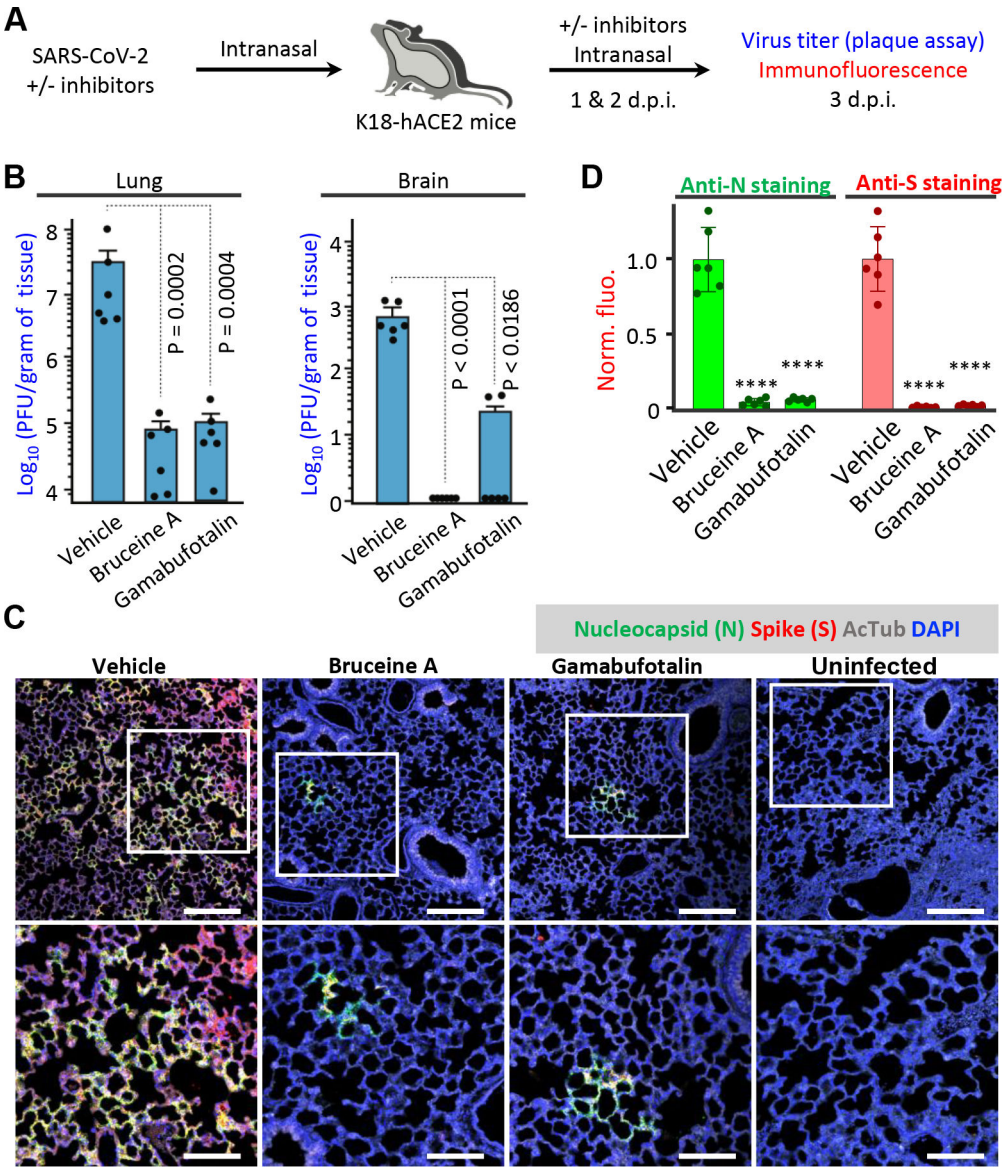

Fig. 6. SARS-CoV-2 infection was inhibited in the mouse models by bruceine A and gamabufotalin.

(**A**) Schematic of the experimental design. K18-hACE2 mice were infected with SARS-CoV-2 (1000 PFU) intranasally with the inhibitors or vehicle control (solvent) at day 0. Then the inhibitors were delivered intranasally once per day at day 1 and 2. At day 3 (i.e., 3 days post infection (d.p.i)), the lung and brain were harvested for analysis. (**B**) Virus titer measurement using plaque assay for the lung and brain. The number of mice is6 (n = 6) per group. Bruceine A and gamabufotalin were used as 3.25 mg/kg by intranasal inoculation. *P* value, two-sided non-paired Welch's t-test between vehicle and treated groups. (**C**) Immunofluorescence images of the lung tissues. The lung slides were stained with antibodies against nucleocapsid protein (N), spike (S), acetylated tubulin (AcTub) and DAPI. Immunofluorescence of N, S, AcTub and DAPI are shown with pseudo-colors green, red, gray and blue, respectively. Lower panels correspond to the boxed areas of the upper

panels. Scalebar, 100 μm (upper panels); 200 μm (lower panels). (**D**) Quantification of the immunofluorescence. The immunofluorescence samples were from 2 mice for each group. Data are shown as mean ± SD. *P* value, two-sided non-paired t-test between vehicle and treated groups. ****P < 0.0001. Exact *P* values: anti-N: bruceine A 7.8E-07, gamabufotalin 5.4E-07; anti-S: bruceine A 8.8E-07, gamabufotalin 6.0E-07.